Flanking Sequence Cotranscriptionally Regulates Twister Ribozyme Activity

Lauren N. McKinley,[1,2] Reuben G. Kern,[2,3] Sarah M. Assmann,[2,4] and Philip C. Bevilacqua[1,2,3,*]

[1]Depatment of Chemistry, Pennsylvania State University, University Park, PA 16802.

[2]Center for RNA Molecular Biology, Pennsylvania State University, University Park, PA 16802.

[3]Department of Biochemistry and Molecular Biology, Pennsylvania State University, University Park, PA 16802.

[4]Department of Biology, Pennsylvania State University, University Park, PA 16802.

Keywords: Small self-cleaving ribozymes, twister ribozymes, flanking sequence, *Oryza sativa*, rice

Abstract

Small nucleolytic ribozymes are RNAs that cleave their own phosphodiester backbone. While proteinaceous enzymes are regulated by a variety of known mechanisms, methods of regulation for ribozymes remain unclear. Twister is one ribozyme class for which many structural and catalytic properties have been elucidated. However, few studies have analyzed the activity of twister ribozymes in the context of native flanking sequence, even though ribozymes as transcribed in nature do not exist in isolation. Interactions between the ribozyme and its neighboring sequences can induce conformational changes that inhibit self-cleavage, providing a regulatory mechanism that could naturally determine ribozyme activity *in vivo* and in synthetic applications. To date, eight twister ribozymes have been identified within the staple crop rice (*Oryza sativa*). Herein, we select several twister ribozymes from rice and show that they are differentially regulated by their flanking sequence using published RNA-seq datasets, structure probing, and co-transcriptional cleavage assays. We found that the Osa 1-2 ribozyme does not interact with its flanking sequences. However, sequences flanking the Osa 1-3 and Osa 1-8 ribozymes form inactive conformations, referred to here as "ribozymogens", that attenuate ribozyme self-cleavage activity. For the Osa 1-3 ribozyme, we show that activity can be rescued upon addition of a complementary antisense oligonucleotide, suggesting ribozymogens can be controlled via external signals. In all, our data provide a plausible mechanism wherein flanking sequence differentially regulates ribozyme activity *in vivo*. More broadly, the ability to regulate ribozyme behavior locally has potential applications in control of gene expression and synthetic biology.

Introduction

RNA adopts a wide variety of structural motifs, allowing it to fulfill critical biological roles including catalyzing peptide synthesis, regulating RNA degradation, and mediating innate immunity.[1] Small self-cleaving ribozymes are catalytic segments of RNA ranging in length from 50 to 150 nt that perform self-cleavage via an internal phosphodiester transfer reaction.[2,3] Thus far, ten classes have been identified including hammerhead,[4] hairpin,[5] HDV,[6] Varkud satellite,[7] *glmS,*[8] HDV-like,[9] twister,[10] twister sister,[11] pistol,[11] and hatchet,[11] with each class defined by a unique structural conformation and catalytic mechanism.

Twister ribozymes have been studied extensively and many of their structural and biochemical properties have been elucidated.[10,12] Structurally, the catalytic core of the twister ribozyme is comprised of three essential pairings, P1, P2, and P4 (Figure 1A), although variants suggest that P1 is dispensable for self-cleavage.[10,13–16] The cleavage site is located between residues –1 and 1 in L1, where residue –1 can be any nucleotide and residue 1 is a conserved A.[10] Self-cleavage occurs via a general acid-base mediated mechanism, in which A1 acts as the general acid and the first G on the 3′ strand of L1 acts as the general base.[10,13–15,17,18] Mutational studies have demonstrated that changes to the general acid and general base are not well-tolerated.[12–14,17,19] The reaction can also be assisted by buffer catalysis under biological reaction conditions.[20] Additionally, ~90% of the twister ribozymes that were initially predicted by Breaker and co-workers possess one or more auxiliary stem-loops, referred to as P3 and P5 (Figure 1A).[10] Even for twister ribozymes with otherwise identical sequences, these auxiliary stem-loops can vary greatly in length and sequence.[10] Finally, the overall structure is compacted by two pseudoknots, PK1 and PK2 (Figure 1A), resulting in a well-defined tertiary structure.[10,13–16]

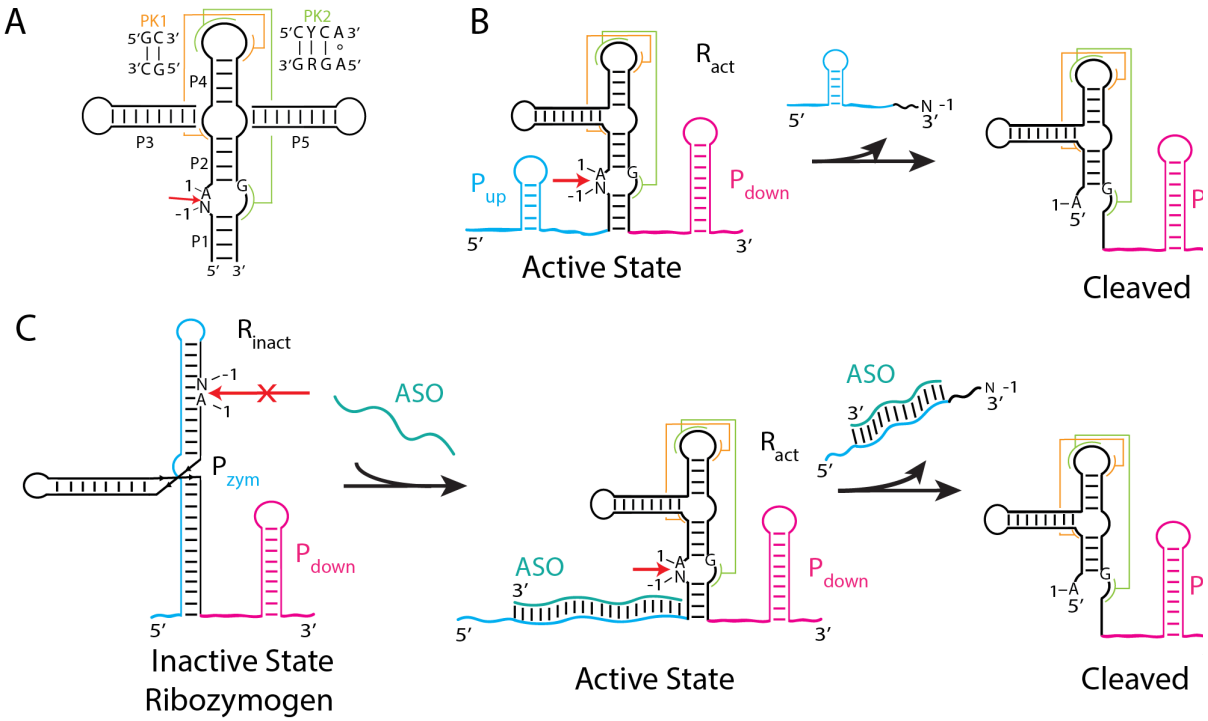

Figure 1. Flanking sequence can differentially regulate ribozyme self-cleavage activity. (A) Secondary structure and tertiary interactions (PK1 and PK2) of a twister ribozyme. The ribozyme structure is drawn according to its consensus structure[10] and characterized crystal structures.[13-16] The cleavage site is designated with a red arrow between N-1 and A1 in L1. The general acid (A1) and general base (G) are shown. (B-C) Upstream and downstream flanking sequences and the ribozyme are colored blue, magenta, and black, respectively. The cleavage site is marked with a red arrow for active ribozymes or with an "x" for inactivated ribozymes. (B) A lack of interactions between flanking regions and the ribozyme promote catalysis by allowing the ribozyme to assume its catalytic structure (R_{act}). Upstream and downstream flanking sequences adopt self-structures P_{up} and P_{down}, respectively. (C) Self-cleavage can be inhibited via interactions between flanking sequences and the ribozyme that create an alternative pairing, P_{zym}, which forces the ribozyme to adopt an inactivated state (R_{inact}) that is a ribozymogen. This inhibition can be relieved by addition of a complementary ASO (teal) that binds to the inhibitory region, here the upstream flank. The ribozyme can then refold to assume its catalytic structure (R_{act}) and self-cleave.

In nature, ribozymes are flanked on both sides by additional nucleotides, which have the potential to base pair with the ribozyme. Despite the existence of such flanking sequences, few studies have assessed how ribozymes are regulated in their native context. Interactions with flanking sequence can disrupt folding of the ribozyme and impair its function by favoring an alternative conformation.[21–26] Alternatively, flanking sequence may not interact with the ribozyme, allowing it to assume its active state and self-cleave.

Indeed, interaction with flanking sequence is a universal mechanism that regulates functional RNAs beyond ribozymes.[21,22] For example, we reported that flanking sequence assists folding of an RNA thermometer in *Bradyhizobium japonicum*, by forming three upstream hairpins that do not interact with the thermometer.[21] In another example, we found that the size and morphology of phase-separated droplets containing G-quadruplexes, a structural motif composed of layered G-quartets, are dictated by the sequences flanking the G-quadruplex.[22] In both large and small ribozymes, regulation by flanking sequence has also been observed. For instance, the activity of the large group I self-splicing intron from *Tetrahymena thermophila* is regulated by flanking sequence in the 5′-exon that disrupts formation of a catalytic stem, preventing self-splicing.[23–25] The same type of regulation occurs for the hepatitis delta virus (HDV) ribozyme, wherein upstream sequence base pairs with the ribozyme, inhibiting native folding and function.[26] The addition of more upstream flanking nucleotides sequester the inhibitory sequence, thereby restoring intrinsic ribozyme activity. In sum, flanking sequence provides a local and potent mechanism for modulating the behavior of diverse functional RNAs.

Twister ribozymes are prevalent across much of life, including bacteria, fish, insects, plants, and reptiles.[10,27] The genome of the staple crop rice (*Oryza sativa*), harbors eight sequences encoding twister ribozymes, named Osa 1-1 through Osa 1-8.[10] Rice is responsible for feeding

over half of the world's population, making it particularly important to study.[28] Unfortunately, rice is susceptible to damage from abiotic stressors as well as pests and pathogens, such as rice blast fungus (*Magnaporthe orzyae*).[29] Indeed, ~30% of rice crops are lost annually due to rice blast, and in severe cases, losses can be as high as 50%.[30,31] Intriguingly, according to the latest gene annotation for rice from Ensembl (Ensembl Annotations release 56), five of the eight rice twister ribozymes have chromosomal locations near one or more putative disease resistance genes.[32] Understanding how twister ribozymes are regulated in rice may thus provide potential new targets for treating rice infected with biotic pathogens such as *M. oryzae.* Moreover, understanding how flanking sequence regulates ribozymes both *in vitro* and *in vivo* is critical for engineering ribozymes for use in synthetic applications like logic circuits and therapeutics.[33,34]

Herein, we report that native flanking sequences differentially regulate the self-cleavage activity of twister ribozymes in rice. We present computational and experimental results on three twister ribozymes including the Osa 1-2 ribozyme which has previously established *in vivo* self-cleavage activity,[10] as well as the Osa 1-3 and Osa 1-8 ribozymes, which are proximal to putative disease resistance genes. First, we determined if these ribozymes are expressed *in vivo*, based on their coverage in published RNA-seq datasets. We then used predictive folding algorithms and in-line probing (ILP) to analyze interactions between the ribozyme and their native flanking sequences. Next, we tested how these interactions impact ribozyme catalysis utilizing co-transcriptional cleavage assays. Each of the three twister ribozymes present a distinct case, with either no, strong, or weak interactions between the ribozyme and neighboring sequences. Overall, our analysis provides insight into the varied effects flanking sequence can have on ribozyme self-cleavage activity.

Methods and Materials

In vivo expression and self-cleavage activity of twister ribozymes in rice

Twister ribozyme sequences were obtained from the initial publication from the Breaker laboratory describing these ribozymes.[10] The presence of the Osa 1-2, Osa 1-3, and Osa 1-8 ribozyme sequences was confirmed in the Os-Nipponbare-Reference-IRGSP-1.0 genome[35,36] using the BLASTn webserver (https://blast.ncbi.nlm.nih.gov/Blast.cgi)[37] where the organism was limited to *Oryza sativa* from the RefSeq database[38] and all other parameters were set to default. Ribozyme chromosome coordinates are provided in Table S1 and are based on the IRGSP-1.0 genome.[35,36] Neighboring sequences and genes were identified in the IRGSP-1.0 genome[35,36] and Ensembl Annotations release 56 for *O. sativa* Japonica group, respectively.[32]

RNA-seq data from rRNA-depleted 10-day old root tissue were downloaded from accession numbers SRR6200382, SRR6200383, and SRR6200476 (151 bp paired-end reads, sequenced on an Illumina HiSeq X Ten). These datasets were chosen because they had a high sequencing depth and included non-polyadenylated RNA. Reads were filtered using fastp (version 0.23.2) to remove reads that were low quality, had multiple unknown bases, or were shorter than 15 nucleotides.[39] Filtered reads were aligned to the rice genome[35,36] using HISAT2 (version 2.2.1)[40] and further filtered to exclude unmapped, supplementary (alignments other than the primary one), and unaligned reads using SAMtools (version 1.17)[41] with flag 2308. Replicates were combined using SAMtools merge.

Coverage per million nucleotides (cpm) for the Osa 1-2, Osa 1-3, and Osa 1-8 ribozymes was calculated using SAMtools depth (version 1.17).[41] To normalize the coverage, read depth at each nucleotide was divided by the total aligned reads and multiplied by one million. Unless otherwise noted, default settings were used for the above programs.

Coverage for the Osa 1-2, Osa 1-3, and Osa 1-8 ribozymes is provided in Figure S1, where ribozymes and flanking sequences are oriented in the 5′ to 3′ direction. Ribozymes were considered to be actively self-cleaving if the coverage between nucleotides -1 and 1 was less than 0.1 cpm.

Conservation of ribozymes and flanking sequences from other rice cultivars and species

To look for single nucleotide polymorphisms (SNPs) in the 3,000 sequenced rice cultivars of *O. sativa*, we used the SNP-seek webserver (https://snp-seek.irri.org/_snp.zul).[42] Datasets were limited to the 3k option for the Variety set and 3k filtered for the SNP set. Genomic coordinates corresponding to the Osa 1-2 and Osa 1-3 ribozymes with 50 nt upstream and 50 nt downstream were input for the region on chromosome 11. All other parameters were default.

To determine if there was conservation of the Osa 1-2 and Osa 1-3 ribozymes and their flanks within other *Oryza* species we searched for similar sequences using the BLASTn webserver (https://blast.ncbi.nlm.nih.gov/Blast.cgi)[37]. Organisms were limited to *Oryza australiensis*, *Oryza barthii*, *Oryza brachyantha*, *Oryza coarctata*, *Oryza glaberrima*, *Oryza glumipatula*, *Oryza longistaminata*, *Oryza meridionalis*, *Oryza meyeriana*, *Oryza minuta*, *Oryza nivara*, *Oryza officinalis*, *Oryza punctata*, and *Oryza rufipogon* from the whole-genome shotgun contigs (wgs) database, and all other parameters remained default. Only species that possessed the Osa 1-2 or Osa 1-3 ribozymes or sequences that closely resembled them were included in our analysis. This resulted in exclusion of 6 species for the Osa 1-2 ribozyme: *O. australiensis*, *O. brachyantha*, *O. coarctata*, *O. meyeriana*, *O. minuta*, and *O. officinalis*. This resulted in exclusion of 7 species for the Osa 1-3 ribozyme: *O. australiensis*, *O. brachyantha*, *O. coarctata*, *O. meyeriana*, *O. minuta*, *O. officinalis*, and *O. punctata*. Those species that did have highly similar sequences to the Osa 1-2 or 1-3 ribozymes were recorded and aligned to *O. sativa* using the Clustal Omega multiple

sequence alignment webserver (https://www.ebi.ac.uk/Tools/msa/clustalo/).[43] Default settings were utilized.

CoFold structure prediction

The CoFold webserver (https://e-rna.org/cofold/), an RNA folding algorithm that takes co-transcriptional folding into account,[44] was used to predict interactions between the rice twister ribozymes Osa 1-2, Osa 1-3, and Osa 1-8 and their respective flanking sequences as they occur co-transcriptionally. The Turner free energy parameters were selected, and all other scaling options were set to default. To mimic RNA interactions that could be produced during transcription, each ribozyme was folded with either 50 nt of native upstream sequence or 50 nt of both upstream and downstream sequences. To generate the secondary structural diagrams, CSV files containing the nucleotide number, RNA sequence, and dotbracket notation output from CoFold were input into the R2easyR package (https://github.com/JPSieg/R2easyR) to create the Stockholm and R2R meta files for R2R, a program that depicts RNA secondary structures.[45]

Antisense Oligonucleotides

To identify potential activating antisense (AS) transcripts from the pathogen rice blast (*M. orzyae*), the 50 nt upstream of the Osa 1-3 ribozyme were input into the BLASTn webserver (https://blast.ncbi.nlm.nih.gov/Blast.cgi).[37] Organisms were limited to *M. orzyae* (taxid:318829) from the RefSeq database,[38] and all other parameters were set to default. Two regions in the *M. oryzae* genome were identified to have extensive complementarity (≥ 95%) to the upstream flanking sequence of the Osa 1-3 ribozyme. These two sequences formed the basis of the 46 nt activating antisense DNA oligonucleotide (ASO) we employed in this study (Table S2). The ASO

was DNA since the interaction is simply dependent on base pairing with the RNA. In addition, three control ASOs (Scramble 1, Scramble 2, and dT_{46}) were designed from sequences that would interact with either the upstream flank, downstream flank, or neither flank of the Osa 1-3 twister ribozyme (Table S2). All ASOs were ordered from Integrated DNA Technologies (IDT). Interactions between the activating or control ASOs and the Osa 1-3 ribozyme with either 50 nt of upstream flanking sequence or 50 nt of upstream and downstream flanking sequences were predicted using BiFold from the RNAStructure package using default parameters.[46]

Co-transcriptional cleavage assays

All ribozyme sequences are provided as both their DNA template and RNA transcripts (Table S2). Templates were obtained from Integrated DNA Technologies (IDT) as single-stranded DNA. The DNA templates were prepared as the reverse complement of the following sequences: the ribozyme with the designated number of flanking nucleotides (no flanking sequence, 50 nt of upstream flanking sequence, or 50 nt of upstream and downstream flanking sequences), a GG start sequence that enhances T7 transcription, and the T7 promoter. Folds of all RNAs were predicted using CoFold (see above), which confirmed that the added GG did not alter the predicted fold.

For each construct, 10 μM each of the above DNA template and T7 promoter (TAATACGACTCACTATAG) were denatured at 90 ˚C for 2 min in 25 mM NaCl and annealed at room temperature for ~10 min to provide a hemi-duplex template. Then, the RNA was *in vitro* transcribed in triplicate with trace amounts of [α-^{32}P] ATP under the following conditions: 1 μM hemi-duplex template, 40 mM Tris (pH 8.3), 2 mM dithiothreitol (DTT), 1 mM spermidine, 625 μM ATP, 5 mM CTP, 5 mM UTP, 9 mM GTP, 25 mM $MgCl_2$, 10 μCi of [α-^{32}P] ATP (PerkinElmer, 250 μCi), and 10% w/v recombinant T7 RNA polymerase (prepared in-house). The

concentration of unlabeled ATP was lowered to enhance the fraction of labeled ATP incorporated into the transcript, and the concentration of GTP was raised to improve the efficiency of transcription initiation.[47] The NTP solutions were adjusted to pH 8.3 using 1 M Tris base before being used in transcription. In some assays, activating or control DNA ASO was added to the transcription mixture to 10 μM final concentration without annealing. All reactions were initiated with T7 polymerase and incubated for 3 h at 30 ˚C, which is a temperature at which rice is typically grown.[48] Timepoints (2 μL) were taken at 30, 60, and 180 min, with aliquots quenched in 18 μL of formamide loading buffer (95% formamide, 50 mM EDTA, 0.1X TBE, 0.1% w/v xylene cyanol, and 0.025% w/v bromophenol blue), and placed on ice. From each timepoint, 5 μL was fractionated by polyacrylamide gel electrophoresis (PAGE) on a 10% denaturing (8.3 M urea) gel run at 20 W for ~1.5 h. After drying, the gels were imaged using a Phosphorimager (Typhoon 650, GE Healthcare), and the 5′- and 3′-cleavage fragments and full-length ribozyme were quantified using ImageQuantTL (version 8.2). Fraction cleaved (f_{cleaved}) was calculated according to equation 1:

$$f_{cleaved} = \frac{I_{CL}}{I_{CL} + I_{FL}} = \frac{I_{5'} + I_{3'}}{I_{5'} + I_{3'} + I_{FL}} \quad \textbf{(1)}$$

where I_{CL}, $I_{5'}$, $I_{3'}$, and I_{FL} are the background-subtracted intensities of the cleaved, 5′- and 3′-cleavage fragments and full-length transcripts, respectively. For each timepoint, f_{cleaved} was averaged across three replicates. Significance of differences in f_{cleaved} for the Osa 1-2, Osa 1-3, and Osa 1-8 ribozymes with different amounts of flanking sequences were determined using Brown-Forsythe and Welch ANOVA tests, which account for the standard deviations being non-uniform across all constructs. This was followed by Dunnett's T3 multiple comparisons post hoc tests to

provide the specific degree of significance between constructs at each timepoint. Resulting P values are reported in Table S3.

In-line probing of RNA secondary structure

In-line probing was performed on the Osa 1-2 and Osa 1-3 ribozymes with 50 nt of upstream sequence. We elected not to study the Osa 1-8 upstream+ribozyme construct using ILP. While CoFold predicted interactions between the ribozyme and its flanking sequence, co-transcriptional cleavage assays nonetheless showed robust self-cleavage activity of the Osa 1-8 upstream+ribozyme construct. As such, the Osa 1-8 upstream+ribozyme construct was not used for ILP.

Constructs for ILP were designed similarly to those for co-transcriptional cleavage assays with the following exceptions: an A1G transition variant was utilized to minimize self-cleavage activity, and a GGA start sequence was used in place of GG to assist in accessibility of the 5′-end for radiolabeling. Neither sequence change was predicted by CoFold to alter the secondary structure of the constructs. All sequences were ordered from Integrated DNA Technologies (IDT) as single-stranded DNA and are listed in Table S2 as their DNA templates and RNA transcripts.

To prepare the RNA for ILP, 10 μM DNA template and T7 promoter were denatured at 90 ˚C for 2 min in 25 mM NaCl and annealed at room temperature for ~10 min to provide a hemi-duplex template. Large-scale transcriptions used 1 μM hemi-duplex DNA template, 40 mM Tris (pH 8.3), 2 mM DTT, 1 mM spermidine, 4 mM ATP, 4 mM CTP, 4 mM UTP, 8 mM GTP, 25 mM $MgCl_2$, and 6% w/v recombinant T7 RNA polymerase (prepared in-house). Reactions were incubated at 37 ˚C for 3 h. The NTP solutions were pH-adjusted to 8.3 as described above, and the concentration of GTP was raised to improve the efficiency of transcription initiation.[47] An

additional 6% w/v of T7 polymerase was added to the samples 1.5 h after initiation of the reaction. The reactions were quenched using an equal volume of 2X formamide loading buffer (95% formamide, 80 mM EDTA, 0.1X TBE, 0.05% w/v bromophenol blue). Afterwards, the transcribed RNA was fractionated using PAGE with a 10% denaturing (8.3 M urea) gel run at 40 W for 4 h and visualized using UV shadowing. The resulting bands were excised from the gel, crushed, and soaked in TEN_{250} (10 mM Tris pH 7.5, 1 mM EDTA, 250 mM NaCl) overnight at 4 ˚C before being ethanol precipitated the next day. Excess salts were subsequently removed using a 3K Amicon Ultra centrifugal filter and rinsing with water.

To remove the 5′-terminal triphosphate from the transcribed RNA, 100 pmol of each transcript was treated with shrimp alkaline phosphatase (SAP, New England Biolabs) for 30 min at 37 ˚C, followed by heat inactivation at 65 ˚C for 5 min. To add a 5′-terminal radioactive phosphate, 10 pmol of the SAP-treated RNA was incubated with [γ-^{32}P] ATP (PerkinElmer, 5 mCi) and T4 polynucleotide kinase (T4PNK, New England Biolabs) at 37 ˚C for just 30 min to minimize ribozyme self-cleavage. Reactions were quenched using an equal volume of 2X formamide loading buffer and fractionated by PAGE using a 10% denaturing (8.3 M urea) gel run at 20 W for 60 min. Bands were excised from the gel and crushed and soaked overnight in TEN_{250} at 4 ˚C, ethanol precipitated the following day, and resuspended in 100 µL of water.

The radiolabeled RNA was refolded by incubating it at 90 ˚C for 2 min and equilibrating at 30 ˚C for 10 min. The ILP reactions were conducted by incubating 1.0 x 10^6 counts per minute per µL (cpm/µL) 5′-end labeled RNA, 40 mM Tris (pH 8.3), 40 mM KCl, 10 mM $MgCl_2$, and 0.01% sodium dodecyl sulfate (SDS) at 30 ˚C for 48 h, which mimics conditions from co-transcriptional cleavage assays; trace SDS was added to inactivate any RNases. The ILP reaction was repeated in triplicate for each transcript. Aliquots (10 µL) were removed at 0, 6, 24, and 48 h

and quenched in 10 μL of 2X formamide loading buffer. At each timepoint for each replicate, 4 μL of the aliquot was fractionated using PAGE on a 10% denaturing (8.3 M urea) gel run for 4 h at 70 W. After drying, the gels were imaged using a Phosphorimager (Typhoon 650, GE Healthcare). The gels were analyzed in triplicate utilizing semiautomated footprinting analysis (SAFA) software.[49] Raw signal for the upstream 50 nt of the Osa 1-2 ribozyme was normalized to the average ILP signal of loop nucleotides -33 to -26, as they were predicted to be single stranded. Similarly, raw signal for the Osa 1-3 ribozyme and its upstream 50 nt was normalized to the average ILP signal of nucleotides -1 to 4, as these nucleotides were predicted to be single-stranded. Calculated ILP signal was mapped onto the appropriate predicted secondary structure using the R2easyR package (https://github.com/JPSieg/R2easyR) and R2R[45] as described above, with the addition of a column in the CSV file containing the ILP signal.

Thermal denaturation (melts)

To assess potential interactions between sequences flanking the Osa 1-3 ribozyme and ASOs, we utilized thermal denaturation, or melts. The upstream flank RNA consisted of 50 nt upstream of the ribozyme as well as the 5′-cleavage fragment (5 nt), while the downstream flank RNA consisted of 50 nt downstream of the 3' end of the ribozyme, and both RNAs were obtained from Integrated DNA Technologies (IDT). The ribozyme sequence was not included because we were interested in how the flanking sequences interact with ASOs and regulate ribozyme activity.

All DNA ASOs and RNA flanks (upstream or downstream) were individually resuspended to a final concentration of 100 μM in water and dialyzed using a 3K Amicon Ultra centrifugal filter into 40 mM MOPS (pH 7.0) and 40 mM NaCl to mimic conditions from the co-transcriptional cleavage assays. Tris (pH 8.3) was replaced with MOPS (pH 7.0) because its pK_a is less sensitive

to temperature.[50] For melts of a single element, either 2 μM ASO (dT_{46}, Scramble 1, Scramble 2, or Activating ASO) or 2 μM flank (upstream or downstream flank) was used. For melts of the mixture, 0.5 μM flank and 1 μM ASO were used at this 1:2 ratio. These concentrations were chosen to provide an optimal absorbance of ~1.0 at 260 nm. Prior to melts, samples were denatured for 2 min at 90 ˚C and allowed to cool to room temperature for ~10 min, at which time $MgCl_2$ was added to a final concentration of 10 mM.

All melts were acquired from 200-600 nm on an HP 8452 diode array, refurbished by OLIS Inc. Absorbances were measured from 5-95 ˚C at increments of 0.5 ˚C with a ramp rate of 0.5 ˚C/min. Raw absorbances for all melts were buffer subtracted. First derivative plots were prepared from the buffer-corrected melt data at 260 nm using a 0^{th} order smoothing polynomial and 3-point smoothing (Prism 9, version 9.5.1). All melting transitions were complete and baselines established by 80 ˚C, so plots were truncated at that temperature. Melting temperatures (T_m) were estimated from the local maximum in the first derivative plots.

To confirm binding of flank and ASO, difference melts were calculated. Concentration-corrected absorbances of 2 μM flank and of 2 μM ASO were subtracted from absorbances of a mixture of 0.5 μM flank and 1 μM ASO. Specifically, the difference melt (Diff Melt) was calculated according to equation 2:

$$\text{Diff Melt} = [0.5\ \mu\text{M flank} + 1\ \mu\text{M ASO}] - 0.25[2\ \mu\text{M flank}] - 0.5[2\ \mu\text{M ASO}] \quad \textbf{(2)}$$

The first derivative of Diff Melt was then taken as described above. Negative peaks in the difference plots indicate loss of free flank and of ASO and thus binding of ASO and flank to each other. Likewise, positive peaks in the difference plots indicate the formation of ASO-bound flank, again indicating binding of ASO and flank to each other. In contrast, the absence of peaks in the difference plots indicates a lack of interaction between ASO and flank.

Results

Flanking sequence can influence ribozyme self-cleavage efficiency. For instance, sequences adjacent to the ribozyme can adopt self-structures that permit the ribozyme's active conformation (R_{act}) and self-cleavage activity. We refer to flanking self-structures within the upstream and downstream sequences as "P_{up}" and "P_{down}", respectively (Figure 1B). Alternatively, flanking sequences may inhibit self-cleavage by base pairing with the ribozyme sequence. Such interactions can produce alternative conformations wherein the ribozyme is instead trapped in an inactivated state (R_{inact}) (Figure 1C). We name such ribozymes "ribozymogens", a portmanteau of "ribozyme" and "zymogen". Similar to protein zymogens, ribozymogens can be activated by binding of an external factor that allows the ribozyme to refold.[51,52] For ribozymes, one such activating factor could be an ASO that has complementarity to the inhibitory region of the flank; binding of the ASO to this inhibitory region would allow the ribozyme to refold into R_{act} and self-cleave (Figure 1C). In the following sections, we provide evidence that native flanking sequence can allow the function of some rice twister ribozymes and inhibit the function of others.

The Osa 1-2 ribozyme self-cleaves efficiently in the presence of its flanking sequences

The Osa 1-2 ribozyme (Figure 2A) has previously been demonstrated to self-cleave *in vitro* and *in vivo*.[10] To establish *in vivo* self-cleavage activity, Breaker and colleagues used an RT-PCR amplification assay with primers that spanned the cleavage site.[10] As an alternative to this assay, which relies on an absence of signal, we examined *in vivo* self-cleavage activity by analyzing the coverage of transcriptome-wide RNA-seq data from 10-day old rice root tissue. RNA-seq reads

were downloaded from the SRA database and mapped to the genome of *O. sativa* Japonica group. Coverage was determined from 6000 nt upstream to 1000 nt downstream of the cleavage site of the ribozyme. Analysis of the aligned data revealed continuous coverage ranging from the upstream gene (*Os11g0139700*, function unknown) to the cleavage site (Figure S1A). Coverage at the cleavage site exhibited a sharp drop to 0 cpm (Figure S1B), indicative of complete self-cleavage of the ribozyme. Indeed, there was very low coverage downstream of the cleavage site (Figure S1A, B), which could suggest that the 3′-cleavage fragment is degraded following self-cleavage. Overall, our RNA-seq analysis provides direct support that the Osa 1-2 ribozyme is expressed and cleaving *in vivo*, as previously reported from loss of RT-PCR signal.[10]

Based on this strong *in vivo* self-cleavage activity, we hypothesized that a lack of interaction between the Osa 1-2 ribozyme and its native flanking sequences permits the ribozyme to fold and self-cleave co-transcriptionally. To evaluate this hypothesis, we folded the Osa 1-2 ribozyme with 50 nt immediately upstream of the ribozyme using CoFold. This predictive RNA folding program takes co-transcriptional folding of the RNA into account, which is necessary since twister ribozymes fold *and* self-cleave while being transcribed.[10,44] No interactions between the ribozyme and its upstream flanking sequence were uncovered by CoFold; indeed, the upstream region adopted a simple hairpin structure (P_{up}) (Figure 2B, blue), while the ribozyme formed its catalytically active structure (R_{act}) (Figure 2B, black). Similar results were obtained when the Osa 1-2 ribozyme was folded with both its upstream and downstream flanking sequences, where formation of P_{up} and the ribozyme as R_{act} were maintained, while the downstream flank formed a hairpin (P_{down}) (Figure 2B, magenta).

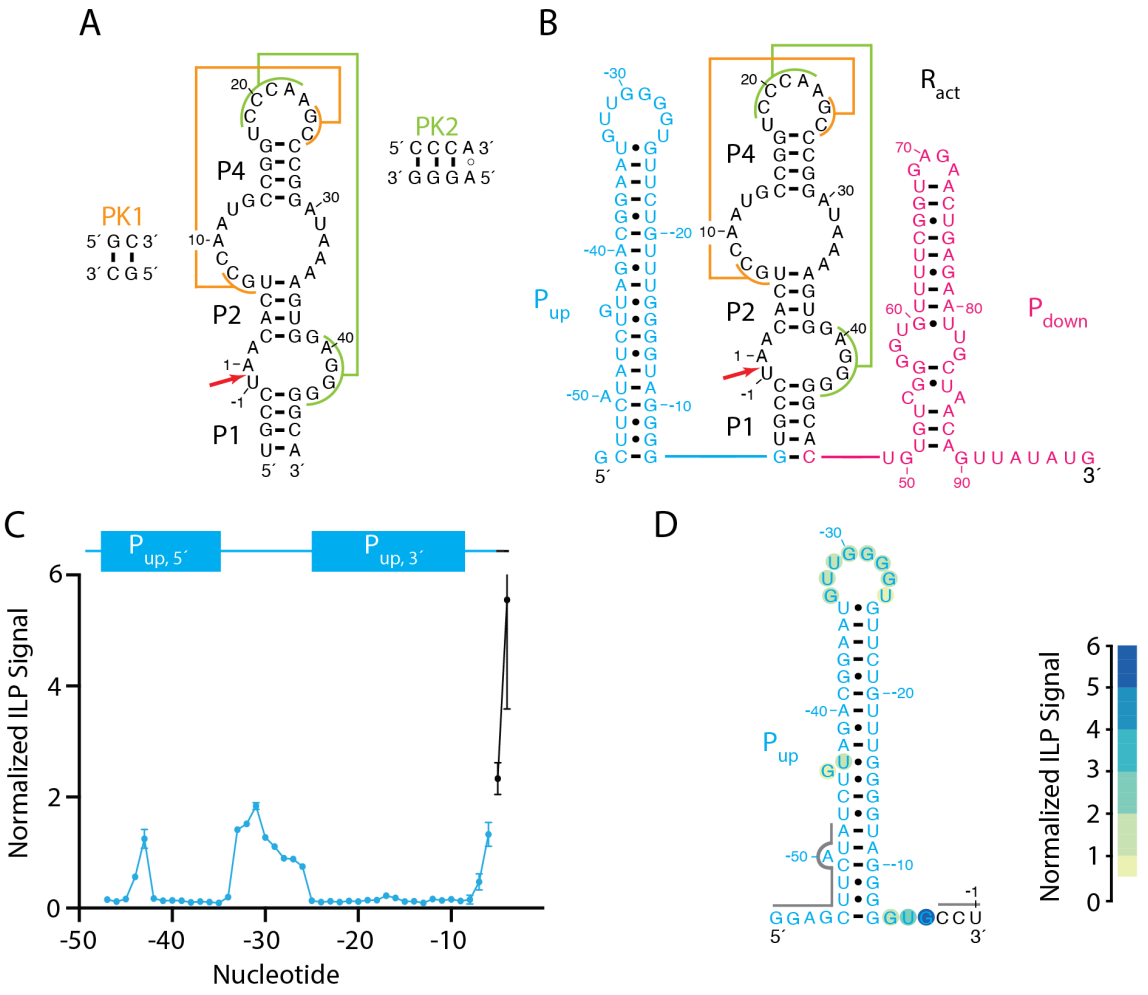

Figure 2. Sequences flanking the Osa 1-2 twister ribozyme do not interact with the ribozyme. (A) Secondary structure of the Osa 1-2 ribozyme. The red arrow indicates the cleavage site, and the specific base pairing interactions of the two pseudoknots, PK1 (orange) and PK2 (green) are shown. (B) Predicted secondary structure of the Osa 1-2 ribozyme (black) with 50 nt upstream (blue) and downstream (magenta). R_{act} is the ribozyme in its active conformation. Without the downstream flank, formation of P_{up} and R_{act} is still maintained (not shown). (C) Normalized ILP signal from 24 h on the predicted hairpin P_{up} upstream of the Osa 1-2 ribozyme. The hairpin was 5´-end labeled and ILP signal was normalized to the average signal of loop nucleotides -33 through -26. There is no signal for -58 to -48 and -3 to -1 since they could not be resolved on the gel or could not be measured with SAFA. Structural features are marked above the graph, with largely paired elements denoted with boxes and single-stranded regions with lines. (D) Normalized ILP signal (24 h) mapped onto the secondary structure for P_{up}. Nucleotides are shaded according to ILP signal and those with a grey line had no signal. Values below 0.5 were not mapped.

We next sought to test this folding model experimentally. First, we determined the secondary structure of the Osa 1-2 upstream+ribozyme construct using ILP, which assesses RNA secondary structure by exploiting hydrated magnesium hydroxide-assisted degradation of single stranded and other flexible regions of the RNA.[53] We attempted to minimize self-cleavage of the Osa 1-2 upstream+ribozyme construct via an A1G transition.[14,17,18] However, despite this mutation, the ribozyme cleaved to completion during transcription. We were, however, able to isolate and probe the 5′-cleavage fragment, which contains P_{up}. This structure is of interest because the *in vivo* self-cleavage activity of the Osa 1-2 ribozyme in the presence of its flanking sequences indicates that the ribozyme is not inhibited by this upstream sequence.[10]

The upstream fragment was studied by ILP under conditions that simulated *in vitro* transcription. The temperature was set at 30 ˚C, which is a typical growth temperature for rice.[48] Timepoints were taken at 0, 6, 24, and 48 h and analyzed for degradation by denaturing PAGE (Figure S2). Nucleotides -50 to -4 were analyzed from the 24 h timepoint, which was the first timepoint to show strong cleavage from ILP, and the signal was normalized over the average signal of residues -33 to -26, which were predicted to be single stranded. After normalization, ILP signal localized primarily to three regions: -44 to -43, -33 to -26, and -6 to -4 (Figure 2C). The ILP signals mapped onto single stranded regions of the CoFold-predicted secondary structure for P_{up}, including all of L_{up} (Figure 2D), supporting the predicted structure. The only exception was nucleotide -43, which was predicted to form a U•G wobble, preceded by a bulged G and another U•G wobble. The high ILP signal of nucleotide -43 is thus attributable to breathing within the RNA structure. Overall, our experimental data strongly support the CoFold predictions.

To further investigate the impact of flanking sequence on the self-cleavage activity of the Osa 1-2 ribozyme, we performed co-transcriptional cleavage assays. Without flanking sequence,

the $f_{cleaved}$ was 0.72 at 30 min for the Osa 1-2 ribozyme, which remained relatively unchanged over the course of the reaction (Figure 3, S3A). Such strong self-cleavage activity is unsurprising as the Osa 1-2 ribozyme conforms to the consensus sequence for active twister ribozymes.[3,10] Similarly, the Osa 1-2 upstream+ribozyme and Osa 1-2 upstream+ribozyme+downstream constructs yielded

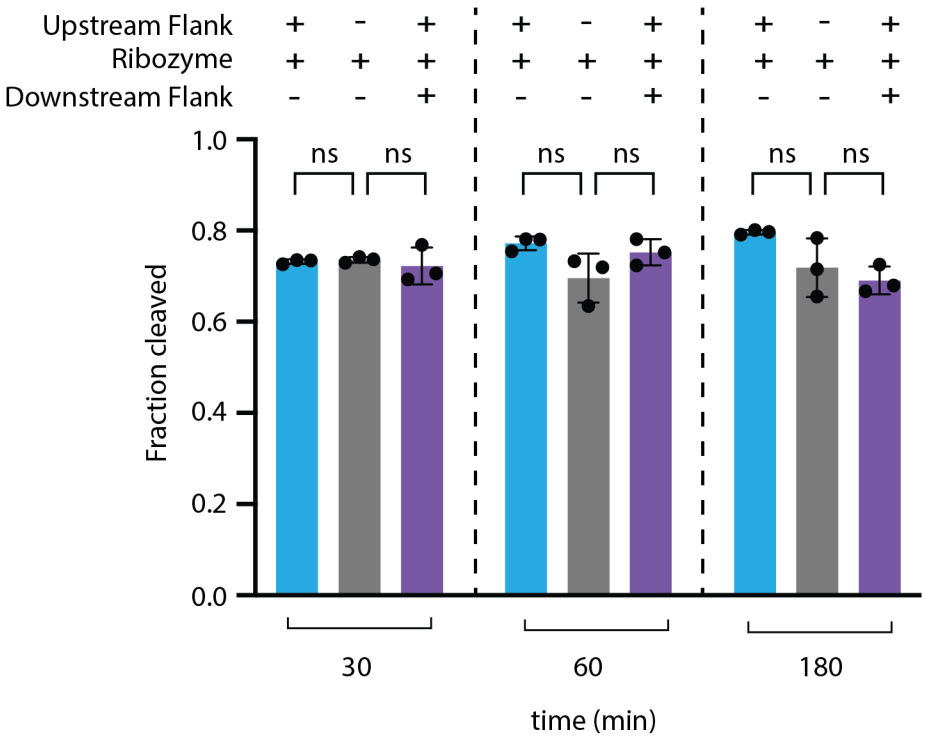

Figure 3. Sequences flanking the Osa 1-2 twister ribozyme do not impede ribozyme self-cleavage. The fraction cleaved for the Osa 1-2 ribozyme with 50 nt upstream (blue), no flanking sequences (gray), and 50 nt upstream and downstream (purple) from co-transcription- al cleavage assays at 30 ˚C. Each construct was body labeled and tested in triplicate. Circles on the graph represent individual fraction cleaved measurements. Average values are depicted with error bars showing the standard deviation. For all P-values α = 0.05 (ns: not significant).

an $f_{cleaved}$ of 0.73 and 0.74 at 30 min, respectively, which were very close to the $f_{cleaved}$ value of 0.72 for the Osa 1-2 ribozyme alone (Figures 3, S3B, & S3C). Indeed, there was no significant difference in the $f_{cleaved}$ value among the three constructs at any timepoint, as substantiated by Brown-Forsythe and Welch ANOVA tests (P values are summarized in Figure 3 and provided in Table S3). Therefore, sequences flanking the Osa 1-2 ribozyme had no significant impact on the ability of the ribozyme to self-cleave, as supported by co-transcriptional self-cleavage assays.

To determine if there was conservation of the Osa 1-2 ribozyme and its flanks, we assessed sequences across the 3,000 sequenced rice cultivars and other *Oryza* species. The SNP-seek database was first searched to look for SNPs in the Osa 1-2 ribozyme and its flanking sequences amongst 3,000 rice cultivars. Only one SNP was found, which was a C-to-G transversion at nucleotide 48, and is predicted to be at the base of P1 (Figure 2B), which has been experimentally shown to be unnecessary for self-cleavage.[15] Moreover, this SNP occurred with a minor allele frequency (MAF) of just 1.99% in the 3,000 cultivars.[42] Interestingly, when separately assessing the 150 cultivars in the aromatic subgroup of rice that are present in the 3k dataset, the allele frequency for this SNP was much higher, at 52.67%.[42] Expanding the search, we then looked at related *Oryza* species that also contained the Osa 1-2 ribozyme. For six other *Oryza* species containing the Osa 1-2 ribozyme, the upstream region was the same as that of *O. sativa*, while in two other species, *O. meridionalis and O. punctata*, the sequence differed by only two to three nucleotides, respectively (Figure S4A). When folded with CoFold, a similar P_{up} was predicted to form for all eight species. In these same eight species, the Osa 1-2 ribozyme itself had 100% sequence similarity to that of *O. sativa* (Figure S4B). For six of the eight species, the downstream region was also highly similar to that of *O. sativa* (Figure S4C). However, both *O. meridionalis*

and *O. punctata* had a large insertion after nucleotide 50 (the third nucleotide of the downstream flank), which was also predicted by CoFold to adopt a strong self-structure.

The Osa 1-3 ribozyme self-cleavage is inhibited by interactions with its flanking sequences

Expanding our analysis, we next studied interactions between the Osa 1-3 ribozyme (Figure 4A) and its flanking sequences. The Osa 1-3 ribozyme is located on chromosome 11, which harbors many putative disease resistance genes,[54] and is flanked by two such genes, *Os11g0673600* and *Os11g0673900* (Table S1). To determine if the Osa 1-3 ribozyme was expressed with its flanking sequences, we analyzed RNA-seq data from 6000 nt upstream to 1000 nt downstream of the cleavage site of the ribozyme. The region upstream of the Osa 1-3 ribozyme was transcribed, including *Os11g0673600* (Figure S1C). The Osa 1-3 ribozyme was also expressed and notably there was a large decrease in coverage at the cleavage site, although not quite to 0 cpm (Figure S1D). Indeed, some of the reads included the ribozyme *and* its upstream and downstream sequences at a level of 0.07 cpm at the cleavage site, suggesting that the ribozyme may not self-cleave to completion *in vivo*.

To ascertain if the Osa 1-3 ribozyme (Figure 4A) interacts with its native flanking sequence, we folded it with 50 nt of its upstream sequence using CoFold. In contrast to the Osa 1-2 ribozyme, with the exception of P3, formation of R_{act} is almost entirely disrupted for the Osa 1-3 ribozyme by its upstream flank. A pairing, hereafter referred to as "P_{zym}" for zymogen pairing, is formed between the pyrimidine-rich upstream region (-36 to -8) and the purine-rich 3′-half of the ribozyme (44 to 73) (Figure 4B, blue and black). This set of interactions appears to lock the ribozyme into an inactivated ribozymogen state, R_{inact}. Next, the Osa 1-3 ribozyme was folded with 50 nt of upstream and downstream flanking sequences using CoFold. Formation of "P_{zym}" and P3

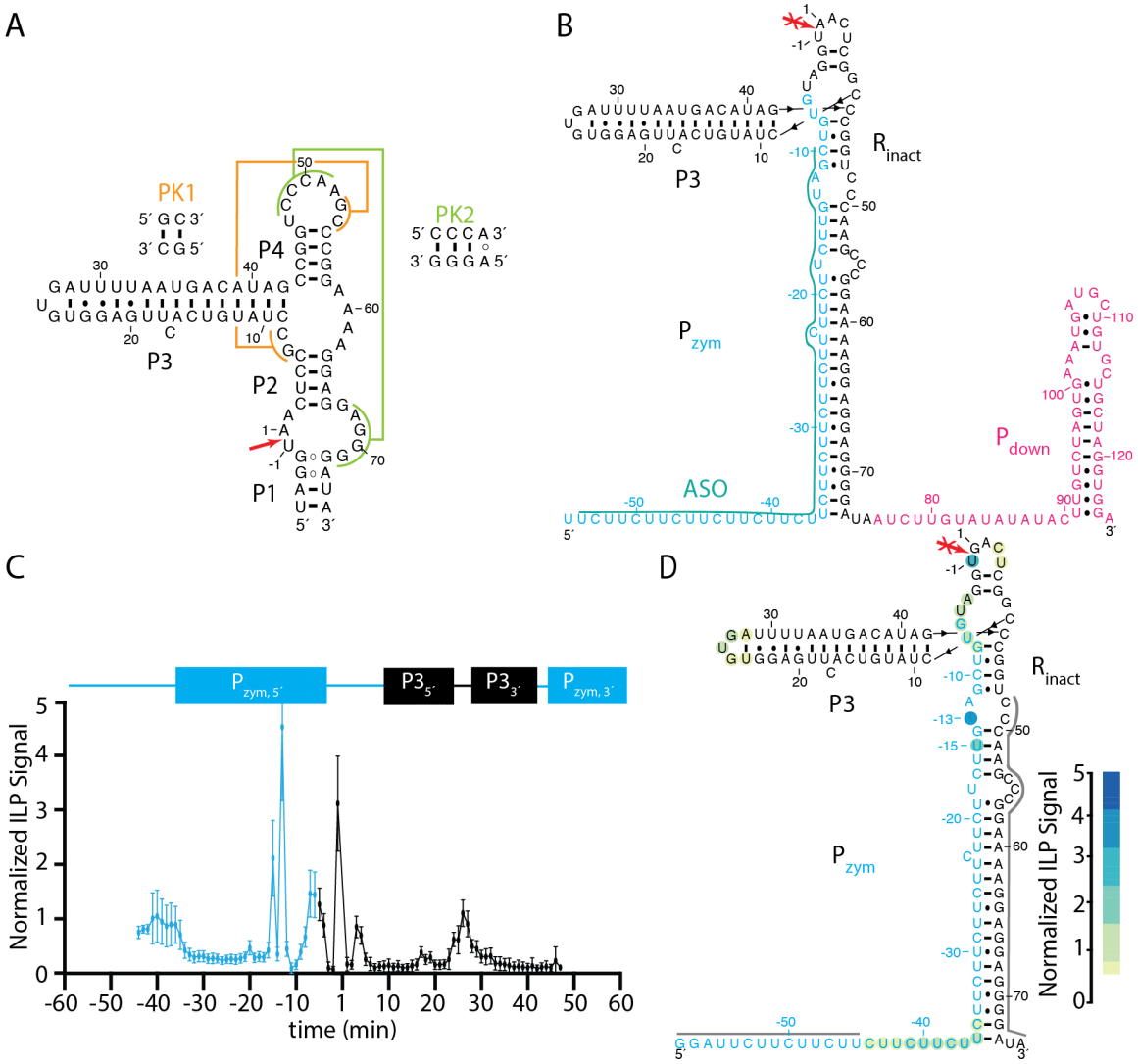

Figure 4. Sequences flanking the Osa 1-3 twister ribozyme interact with the ribozyme. Colors match those used in Figure 2. (A) Secondary structure of the Osa 1-3 ribozyme. The red arrow indicates the cleavage site, and the specific base pairing interactions of the two pseudoknots PK1 (orange) and PK2 (green) are shown. (B) Predicted secondary structure of the Osa 1-3 ribozyme with 50 nt upstream and downstream, with the ribozyme forming $P_{zymogen}$ (P_{zym}). The red arrow with an "x" indicates the cleavage site in the inactivated state (R_{inact}), and the teal line is where the complementary activating ASO binds. (C) Normalized ILP signal from 24 h on the Osa 1-3 ribozyme with 50 nt upstream. This construct was 5′-end labeled and ILP signal was normalized to the average signal of nucleotides -1 to 4. There is no signal for -58 to -45 and 48 to 75 since they could not be resolved on the gel or measured by SAFA. Structural features are marked above the graph, with largely paired elements denoted with boxes and single-stranded regions with lines. (D) Normalized ILP signal (24 h) mapped onto the predicted secondary structure P_{zym}. Nucleotides are shaded according to ILP signal and those with a grey line had no signal. Values below 0.5 were not mapped.

were maintained, while the sequence downstream of the ribozyme (91 to 124) adopted a small

pairing "P_{down}" (Figure 4B, magenta).

To test the secondary structure of the Osa 1-3 upstream+ribozyme construct, we again employed ILP under conditions that simulated *in vitro* transcription. As with the Osa 1-2 ribozyme, we utilized an A1G mutant to minimize self-cleavage, and here we were able to isolate the full-length transcript containing the Osa 1-3 ribozyme and upstream flank. We then performed ILP (Figure S5) as described above. Nucleotides -44 to 47 were quantified and ILP signal was normalized to the average signal of nucleotides -1 to 4, which were predicted to be single-stranded.

Analysis of the ILP data revealed several regions of high signal for the Osa 1-3 upstream+ribozyme construct (Figure 4C). For instance, nucleotides -44 to -35 displayed normalized ILP signals near 1.0 and aligned with the unstructured 5′-stretch of the predicted structure (Figure 4D). Intriguingly, nucleotides -15 and -13 had high signals of 2.1 and 4.5, respectively (Figure 4C). While expected for nucleotide -13, as it is part of an internal bulge within the predicted structure (Figure 4D), nucleotide -15 was predicted to form an AU base pair with 51 (Figure 4D). It is plausible that nucleotide -15 may be somewhat dynamic and not form a base pair. Further downstream, residues -8 through -4 had high ILP signals (Figure 4C), which corresponded well with an internal loop and its closing base pair within the predicted secondary structure (Figure 4D). In the topmost loop of the structure (Figure 4D), nucleotides -1, 3, and 4 had average ILP signals of 3.1, 1.0 and 1.0, respectively, supporting the predicted structure (Figure 4C). Nucleotides in L3 (25 to 27) exhibited signals above background, supporting the formation of P3 (Figure 4D). Both residues 24 and 28, which formed the last predicted base pair of P3 (Figure 4D), had similar ILP signal to L3 nucleotides (Figure 4C), suggesting they may not always interact. In general, the highest ILP signals for the Osa 1-3 upstream+ribozyme construct aligned to single-

stranded regions, while nucleotides predicted to base pair had negligible signal. Even though the 3′-most nucleotides in this construct could not be resolved to single nucleotide resolution, there were no dark bands observed near the top of the gel, aside from the remaining full-length construct (Figure S5), supporting predictions that these bases pair with other nucleotides as depicted in Figure 4D. In sum, the ILP data strongly support the structural predictions of a ribozymogen made by CoFold.

From this structural analysis, we predicted that self-cleavage activity of the Osa 1-3 ribozyme would be diminished in the context of its flanking sequences. To test this, we conducted co-transcriptional cleavage assays of the ribozyme with upstream and downstream flanking sequences. In the absence of flanking nucleotides, the Osa 1-3 ribozyme had an $f_{cleaved}$ of 0.65, which remained constant from 30 to 180 min (Figure 5, S6A). This indicated that the ribozyme itself is intrinsically active, consistent with conservation of key nucleotides, including the general acid and general base. Strikingly, when the upstream flank (50 nt) was present in the Osa 1-3 upstream+ribozyme construct, the $f_{cleaved}$ was just 0.10 at 30 min, and rose to only 0.17 at 180 min (Figure 5, S6B), which was significantly different from the ribozyme with no flanking sequence at both timepoints. Furthermore, when the ribozyme had both upstream and downstream flanks (50 nt each) in the Osa 1-3 upstream+ribozyme+downstream construct, the $f_{cleaved}$ was 0.15 at 30 min and remained low at 0.18 at 180 min (Figure 5, S6C), which was also significant compared to the ribozyme with no flanking sequence at both timepoints. The reduced self-cleavage activity of the Osa 1-3 ribozyme in the presence of its upstream flank, even after 180 min, therefore supports formation of P_{zym} as predicted by CoFold and measured by ILP.

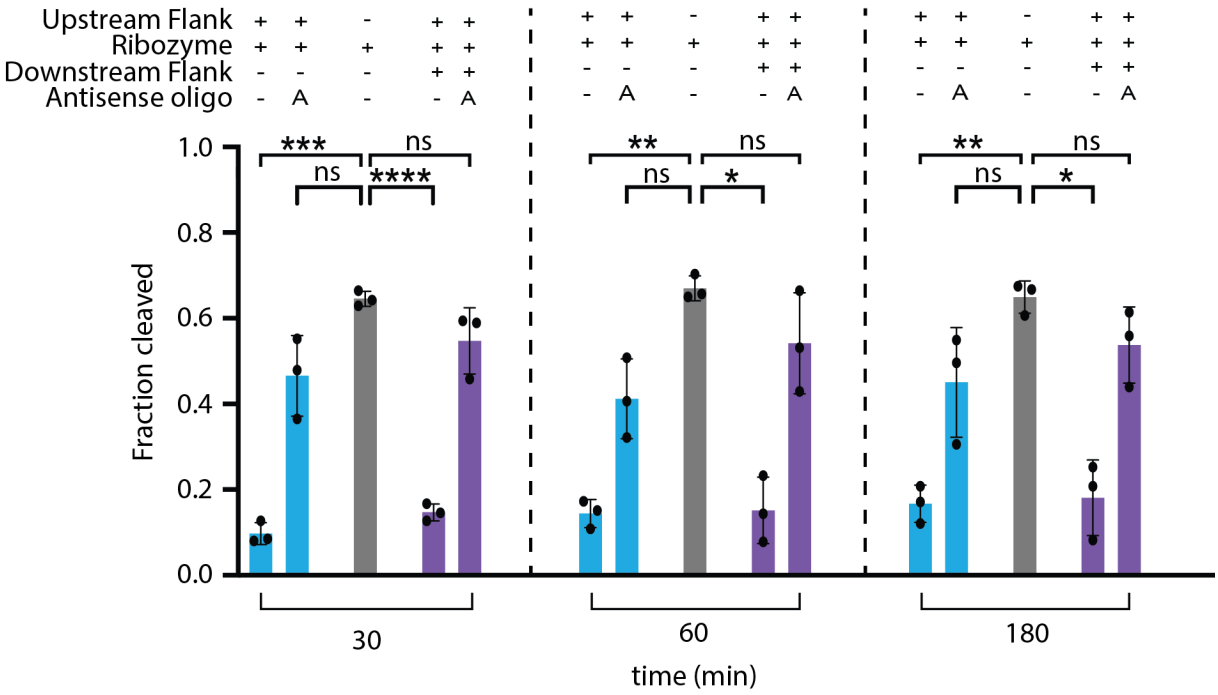

Figure 5. Sequences flanking the Osa 1-3 twister ribozyme inhibit ribozyme self-cleavage. Colors match those used in Figure 3. The fraction cleaved for the Osa 1-3 ribozyme with 50 nt upstream, no flanking sequence, and 50 nt upstream and downstream from co-transcriptional cleavage assays at 30 ˚C. The activating ASO is denoted as "A". Each construct was body labeled and tested in triplicate. Circles on the graph represent individual fraction cleaved measurements. Average values are depicted with error bars showing the standard deviation. For all P-values α = 0.05 (ns: not significant; *: P ≤ 0.05; **: P ≤ 0.01; ***: P ≤ 0.001; ****: P ≤ 0.0001).

We then looked at conservation of the Osa 1-3 ribozyme and its flanks in the 3,000 sequenced rice cultivars or other *Oryza* species. Using the SNP-seek database of the 3,000 sequenced rice cultivars, no SNPs were reported for the Osa 1-3 ribozyme or its flanks. When looking at the upstream flank in other *Oryza* species (seven), similar sequences were found as in *O. sativa* (Figure S7A). Unlike the Osa 1-2 ribozyme, some sequence differences were found for the Osa 1-3 ribozyme itself, in L1, P2, P3 & L3, and P4 (Figure S7B, bottom structural elements). The downstream flank in the other *Oryza* species had similar sequences as in the Osa 1-3 ribozyme from *O. sativa* (Figure S7C). The slight differences in the upstream and downstream flanking

sequences do not affect the CoFold prediction of P_{zym} when the ribozyme and both flanks are folded together.

The Osa 1-3 ribozyme with its upstream 50 nt can be activated by a complementary ASO

Given that the upstream flanking sequence strongly inhibits the intrinsic self-cleavage activity of the Osa 1-3 ribozyme, we assessed restoration of self-cleavage activity by an ASO. We designed an activating ASO using genomic sequences from rice blast *M. oryzae* (Figure S8). We found perfect complementarity between a sequence from rice blast (NC_017844.1, Chr 1: 6501457-6501496, E-value= $1e^{-15}$) and nucleotides -54 to -15 upstream of the Osa 1-3 ribozyme and excellent complementarity between another rice blast sequence (95%, NC_17850.1, Chr 2: 5198116-5198134, E-value= 0.002) and nucleotides -27 to -10 upstream of the Osa 1-3 ribozyme (Figure S8). Moreover, both of these regions in *M. oryzae* were shown to be expressed in transcripts *MG_14329* and *MG_01883*, respectively.[55] The activating ASO used here was designed by overlapping these regions to complement nucleotides -54 to -10 upstream of the Osa 1-3 ribozyme (Figure S8). The binding site for the activating ASO is depicted in Figure 4B by a teal line. We hypothesize that invading nucleic acids, in the form of an ASO, could base pair with and sequester the inhibitory upstream flank of the Osa 1-3 ribozyme. The 5′-unstructured end of the rice transcript, upstream of P_{zym} (Figure 4B), could be used as a toehold[56,57] for initial binding to the transcript. The ASO could then invade into the inhibitory region, P_{zym}, disrupting interactions between the flanking sequence and ribozyme. Such a toehold strategy would obviate the need for high temperature to render P_{zym} accessible for base pairing. Indeed, we added ASOs to our transcription mixtures without heating. Once the inhibitory upstream region was sequestered, the ribozyme could refold into R_{act} and self-cleave. This, therefore, allows for controlled activation of the ribozyme.

To confirm binding of the activating ASO to the upstream flank of the Osa 1-3 ribozyme, we conducted melts. We tested a 1:2 mixture of the upstream flank to activating ASO (Figure 6A), as well as performed melts on the activating ASO alone (Figure 6B) and upstream flank alone (Figure 6C). It was anticipated that binding of the activating ASO to the upstream flank would result in an upward shifted T_m as compared to the T_m for the ASO and for the upstream flank alone. To assess this, we calculated a difference melt in Figure 6D according to equation 2. As expected, when the activating ASO and upstream flank were mixed, there was a large upward shift in the T_m, observed as a major positive peak between 70 and 80 ˚C (Figure 6A). In the difference plot (Figure 6D), a negative peak was found near 40 ˚C that corresponded well with transitions seen in melts of the ASO alone (Figure 6B) and upstream flank alone (Figure 6C). The negative peak represents the depletion of free ASO and upstream flank in the mixture. These observations strongly support binding of the activating ASO to the upstream flank.

We also melted the downstream flank of the Osa 1-3 ribozyme with the activating ASO at a 1:2 ratio, where no interaction between the two was predicted. In the absence of interaction, it was anticipated that the T_m of the mixture and of each single melt would overlap and subtract to zero. The first derivative of the mixture yielded two peaks (Figure 6E), which aligned well with melt transitions for the activating ASO alone (Figure 6F) and downstream flank alone (Figure 6G). In the difference plot (Figure 6H), almost no signal was observed. In sum, the melt data support the activating ASO binding with the upstream flank, but not the downstream flank.

To assess if the activating ASO altered self-cleavage activity, we added it to co-transcriptional cleavage assays of the Osa 1-3 ribozyme with 50 nt of upstream flank or 50 nt of

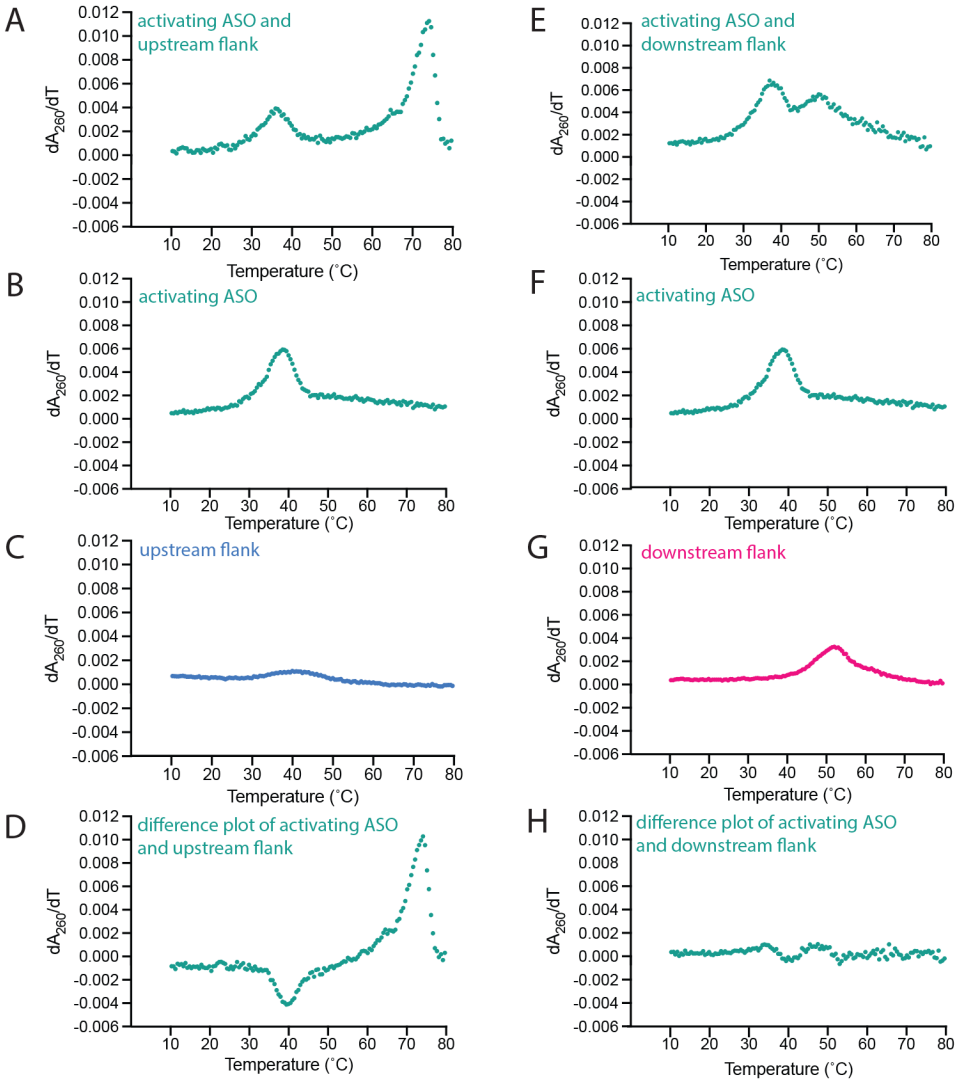

Figure 6. Interactions between the activating ASO and the upstream flank (A-D) and downstream flank (E-H) of the Osa 1-3 ribozyme using thermal denaturation melts. Colors match those used in Figure 4B. Absorbance was measured at 260 nm and buffer subtracted (40 mM MOPS, 40 mM NaCl, 10 mM MgCl2). All melts were conducted in triplicate and the average is shown. Absorbance was divided by 4 for the flanking sequence and by 2 for the activating ASO, prior to taking the first derivative, to account for differences in concentration between single melts and those of mixtures. (A-C) Thermal denaturation first derivative plots of (A) a 1:2 mixture of the upstream flank (0.5 μM) with the activating ASO (1 μM), (B) the activating ASO (2 μM), (C) and the upstream flank (2 μM). (D) First derivative difference plot of the upstream flank- and ASO-subtracted mixture calculated using equation 2. (E-G) Thermal denaturation first derivative plots of (E) a 1:2 mixture of the downstream flank (0.5 μM) with the activating ASO (1 μM), (F) the activating ASO (2 μM), (G) and the downstream flank (2 μM). (H) First derivative difference plot of the downstream flank- and ASO-subtracted mixture calculated using equation 2.

upstream and downstream flank. The Osa 1-3 upstream+ribozyme construct without any ASO had an $f_{cleaved}$ of 0.10 at 30 min, which rose nearly 5-fold, to 0.47, when the activating ASO was present (Figure 5, S9A). Similarly, the Osa 1-3 upstream+ribozyme+downstream construct without any ASO had an $f_{cleaved}$ of 0.15 at 30 min, which rose over 3-fold, to 0.55, when the activating ASO was present (Figure 5, S10A). Overall, addition of the activating ASO resulted in $f_{cleaved}$ values that were similar to those of the Osa 1-3 ribozyme without any flanking sequence (Figure 5), indicating a potent effect of the activating ASO on ribozyme self-cleavage activity.

In addition to the activating ASO, three control ASOs were designed, all the same length as the activating ASO. The first was a dT_{46} strand, which was predicted to not interact with the ribozyme or its upstream and downstream flanks. Melts conducted with dT_{46} and the upstream and downstream flanks, indeed revealed no interaction between these elements (Figure S11). The second control ASO, called "Scramble 1", was a randomization of the activating ASO. Scramble 1 was predicted to bind primarily to the 5′-unstructured end of the upstream flank and partially invade P_{zym} (Figure S12A, teal and blue). Scramble 1 was also predicted to interact with P_{down} (Figure S12A, teal and magenta). Interaction between Scramble 1 and the upstream flank was clearly supported by melts, in which there was a negative peak at a lower temperature followed by a positive peak (Figure S11D). In the case of Scramble 1 and the downstream flank, there were two negative lower temperature peaks but no clear positive peak (Figure S11H). This behavior supports weak and perhaps non-specific interaction of Scramble 1 with the downstream flank. The third ASO, called "Scramble 2", was a randomly generated sequence, which was found to have partial complementarity to the downstream flank (Figure S12B, teal and magenta). Despite these predicted weak interactions, melt data suggested no binding of Scramble 2 to the flanking sequences (Figure S11), perhaps because of the competing self-structure of P_{down}.

We also tested these three control ASOs individually in co-transcriptional cleavage assays with the Osa 1-3 upstream+ribozyme and upstream+ribozyme+downstream constructs. First, dT_{46} was tested with the Osa 1-3 upstream+ribozyme construct, and the $f_{cleaved}$ remained low at 0.14 even after 180 min (Figure S9B, S9C). This value was similar to the $f_{cleaved}$ of 0.17 at 180 min when no ASO was added. Similarly, when dT_{46} was tested with the Osa 1-3 ribozyme with both flanking sequences, the $f_{cleaved}$ was 0.16 after 180 min (Figure S10B, S10C), again similar to the $f_{cleaved}$ of 0.18 at 180 min when no ASO was added. This suggests that dT_{46} has no impact on the self-cleavage activity of both Osa 1-3 constructs with flanking sequences.

The second control ASO, Scramble 1, which interacted with the upstream and downstream flanks (Figure S11, S12A), similarly did not restore self-cleavage activity when added to the co-transcriptional cleavage assays. When Scramble 1 was tested with the Osa 1-3 upstream+ribozyme construct, the $f_{cleaved}$ remained low at 0.10 after 180 min (Figure S9B, S9C), which was similar to the $f_{cleaved}$ of 0.17 at 180 min when no ASO was added. Likewise, when Scramble 1 was tested with the Osa 1-3 ribozyme with both flanking sequences, the $f_{cleaved}$ was 0.18 at 180 min (Figure S10B, S10C), which was the same as the $f_{cleaved}$ when no ASO was added. When analyzed in combination with the melt data, this suggests that Scramble 1 binds to the flanking sequences, but that it does so without significantly disrupting P_{zym}.

The third control ASO was Scramble 2, which did not interact significantly with flanking sequences as indicated by melting data (Figure S11). When Scramble 2 was tested in co-transcriptional cleavage assays with the Osa 1-3 upstream+ribozyme construct, the $f_{cleaved}$ at 180 min increased two-fold from 0.17 when no ASO was present to 0.33 (Figure S9B, S9C). Despite this increase, the extent of reaction was still significantly less than when no flanking sequence was

present (Figure S9C). Indeed, the stimulatory effect of Scramble 2 was lost in the presence of both upstream and downstream flanking sequence (Figure S10B, S10C).

The Osa 1-8 ribozyme is predicted to weakly interact with its flanking sequence

Like the Osa 1-3 ribozyme, the Osa 1-8 ribozyme (Figure 7A) is found on chromosome 11, where it is located between two putative disease resistance genes, *Os11g0674400* and *Os11g0676050* (Table S1). As described above, we analyzed the coverage from transcriptome-wide sequencing data in *O. sativa* taken from 10-day old root tissue. The Osa 1-8 ribozyme and its flanking regions appear to be transcribed in roots and have similar levels of coverage to that of the upstream gene *Os11g0674400* (Figure S1E). As observed with the Osa 1-2 ribozyme, there is a drastic decrease in coverage, down to 0 cpm, immediately at the cleavage site (Figure S1F), suggesting that the Osa 1-8 ribozyme self-cleaves to completion *in vivo*. Unlike the Osa 1-2 ribozyme, however, coverage downstream of the Osa 1-8 ribozyme remains at a similar level to coverage upstream of the ribozyme, suggesting that the 3′-cleavage fragment is protected from degradation.

The Osa 1-8 ribozyme was folded with 50 nt of upstream or 50 nt of upstream and downstream flanking sequence using CoFold. In the predicted structure, formation of R_{act} for the Osa 1-8 ribozyme was partially disrupted when folded with its upstream 50 nt (Figure 7B). Upstream flanking nucleotides -40 to -27 and -14 to -6 formed helices with ribozyme nucleotides 59 to 72 and 5 to 12, respectively. These P_{zym}-containing helices were separated by a 12 nucleotide loop. Here, additional portions of the Osa 1-8 ribozyme remained natively folded, as most of P3 and P4 were predicted to form (Figure 7B). In the presence of both flanking sequences, R_{act} for the Osa 1-8 ribozyme was not predicted to form (Figure 7C). Instead, folding of the ribozyme was

disrupted by base pairing interactions between the 3′-most end of the upstream flank (-34 to -7) and the 3′-end of the

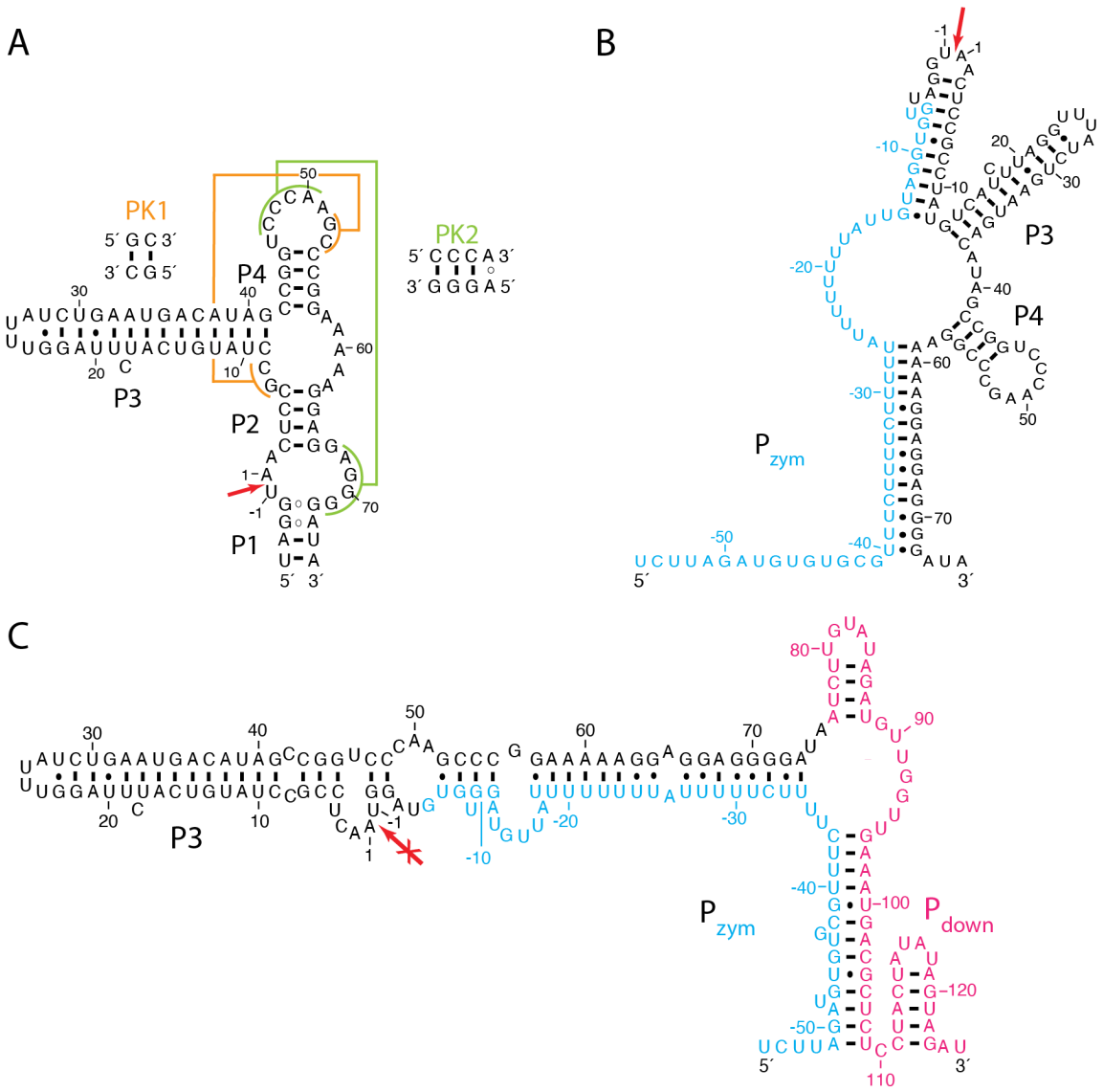

Figure 7. Sequences flanking the Osa 1-8 twister ribozyme are predicted to weakly interact with the ribozyme. Colors match those used in Figures 2 and 4. (A) Secondary structure of the Osa 1-8 ribozyme. The red arrow indicates the cleavage site and the specific base pairing interactions of the pseudoknots PK1 (orange) and PK2 (green) are shown. (B) Predicted secondary structure of the Osa 1-8 ribozyme with 50 nt upstream forming a weak P_{zym}. (C) Predicted secondary structure of the Osa 1-8 ribozyme with 50 nt upstream and downstream, with the ribozyme forming a weak P_{zym}.

ribozyme (52 to 73). Again, part of the Osa 1-8 ribozyme did remain natively folded, as P3 was still predicted to form. Additionally, upstream nucleotides -51 to -37 formed a helix with downstream nucleotides 96 to 109. Those downstream nucleotides that did not base pair with the upstream flank instead self-paired to adopt a small P_{down}. Since sequences flanking the Osa 1-8 ribozyme were predicted to prevent formation of R_{act}, we hypothesized that self-cleavage activity might be inhibited.

To test the functional consequences of flanking sequence on the self-cleavage activity, we conducted co-transcriptional cleavage assays. Without any flanking sequence, the Osa 1-8 ribozyme had an $f_{cleaved}$ of 0.63 at 30 min, rising slightly to 0.69 and 0.72 at 60 and 180 min, respectively (Figures 8, S13A). The Osa 1-8 upstream+ribozyme construct had similar $f_{cleaved}$ values at 30, 60, and 180 min (Figure 8, S13B) to the intrinsically active ribozyme, and only differed significantly at 60 min. From the structural prediction above, it was anticipated that the upstream flank of the Osa 1-8 upstream+ribozyme construct might hinder self-cleavage activity, but the co-transcriptional cleavage assays indicated that any attenuation was minimal.

In the presence of both upstream and downstream flanks, a somewhat lower $f_{cleaved}$ of 0.54 and 0.61 was found at 30 and 60 min, which was significantly different from the ribozyme with no flanking sequence (Figure 8, S13C). However, by 180 min the difference in $f_{cleaved}$ between the upstream+ribozyme+downstream construct and ribozyme alone was negligible (Figure 8). Thus, when both flanking sequences are present, self-cleavage of the Osa 1-8 ribozyme is slightly impeded at earlier timepoints, which is consistent with the inhibitory interactions depicted in Figure 7C.

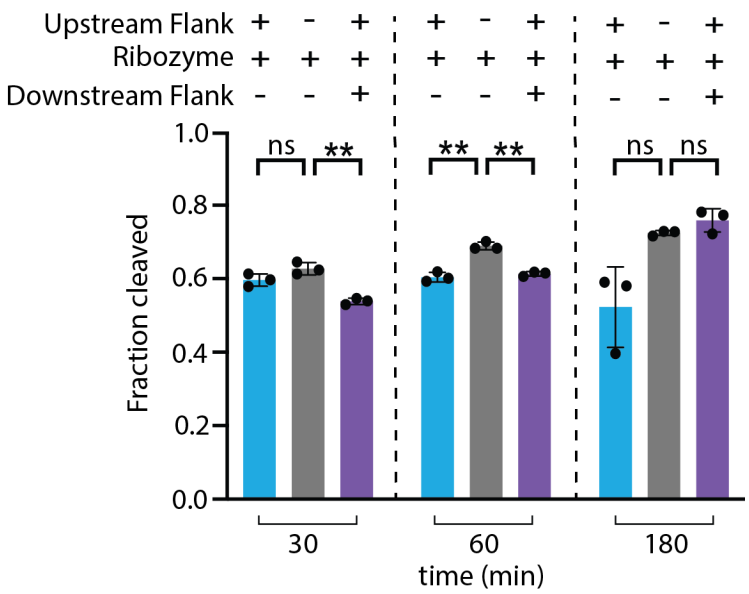

Figure 8. Sequences flanking the Osa 1-8 twister ribozyme minimally inhibit ribozyme self-cleavage. Colors match those used in Figures 3 and 5. The fraction cleaved for the Osa 1-8 ribozyme with 50 nt upstream, no flanking sequence, and 50 nt upstream and downstream from co-transcriptional cleavage assays at 30 ˚C. Each construct was body labeled and tested in triplicate. Circles on the graph represent individual fraction cleaved measurements. Average values are depicted with error bars showing the standard deviation. For all P-values $\alpha = 0.05$ (ns: not significant; *: $P \leq 0.05$; **: $P \leq 0.01$).

Discussion

Nearly all genes are regulated in some fashion. This can occur epigenetically, transcriptionally, post-transcriptionally, or translationally.[58] Here, we provide evidence for co-transcriptional regulation of small ribozymes. We describe one of the simplest ways to regulate such RNAs: through interactions between the ribozyme and its native flanking sequences. We show that native flanking sequences can either not interact, weakly interact, or strongly interact with a neighboring ribozyme depending on the specific case. Indeed, many short RNAs that function in biology (i.e.

ribozymes, riboswitches, RNA thermometers) have this simple but potent mechanism of localized regulation built in.[21,26,59,60]

For small self-cleaving ribozymes, flanking sequences can impact catalysis in two ways. A lack of interactions between the ribozyme and its flanking sequences can permit self-cleavage by allowing the ribozyme to assume R_{act} and react at its intrinsic rate (Figure 1B). Conversely, base pairing interactions between the ribozyme and neighboring flanking sequences can produce alternative conformations that inhibit catalysis (Figure 1C). Herein we considered how flanking sequence differentially impacted catalysis of three rice twister ribozymes; we observed *in vitro* evidence of three distinct cases where flanking sequence either did not inhibit self-cleavage (Osa 1-2), strongly inhibited self-cleavage (Osa 1-3), or mildly inhibited self-cleavage (Osa 1-8).

Previous studies have shown that the Osa 1-2 ribozyme self-cleaves *in vivo*,[10] and here we demonstrate that this may be attributed to a lack of interaction between the ribozyme and its flanking sequences. It is interesting that native flanking sequences achieve a lack of interaction with the ribozyme by forming their own self-structures (Figure 2B, D). As such, the ribozyme is free to assume its catalytically active conformation R_{act} and self-cleave. Indeed, the $f_{cleaved}$ from co-transcriptional cleavage assays of the Osa 1-2 ribozyme with no flanking sequence, the upstream+ribozyme construct, and the upstream+ribozyme+downstream construct displayed negligible differences between these constructs across all timepoints (Figure 3).

In contrast, the Osa 1-3 ribozyme forms stable interactions with its upstream flanking nucleotides that attenuate self-cleavage. When the upstream flank and Osa 1-3 ribozyme were transcribed together, the ribozyme adopted an alternative conformation, P_{zym}, in which the ribozyme assumed a catalytically inactive state R_{inact} (Figure 4B and 4D). Based on this alternative structure, ribozyme self-cleavage activity should be greatly reduced, which was indeed reflected

in the co-transcriptional cleavage assays as the $f_{cleaved}$ at 180 min remained below 0.20 for the Osa 1-3 ribozyme whenever its upstream flank was present (Figure 5). Self-cleavage activity was rescued only when the activating ASO, which has near perfect complementarity to the upstream flank, was added (Figure 5). ASOs have been employed in many applications, including in pharmaceuticals where they have been shown to stop viral replication and are used to treat various neurological disorders.[61,62] Such ASOs could be used to activate ribozymogens in synthetic applications to selectively regulate ribozyme activity under certain conditions.

The position at which the ASO interacts with P_{zym} influences how effective it is at activating the ribozyme. The activating ASO we employed disrupted most interactions between the Osa 1-3 ribozyme and its upstream flank (Figure 4B). On the other hand, Scramble 1 was also shown to bind with the upstream flank of the ribozyme (Figure S11), yet when added to co-transcriptional cleavage assays, it did not increase the $f_{cleaved}$ above 0.20, even after 180 min for both the Osa 1-3 upstream+ribozyme or Osa 1-3 upstream+ribozyme+downstream constructs (Figure S9,S10). This can be attributed to how Scramble 1 interacts with the upstream flank, as it leaves most of P_{zym} undisturbed and thus the ribozyme is still locked in R_{inact}, unable to self-cleave (Figure S12A). Furthermore, specificity is also inherent to the activating ASO, as neither dT_{46} nor Scramble 2 activated the ribozyme (Figure S9,S10). As such, it appears that a somewhat high degree of specificity is needed to activate the Osa 1-3 ribozymogen.

Finally, flanking sequences only marginally impaired ribozyme self-cleavage activity for the Osa 1-8 ribozyme. Here, the Osa 1-8 ribozyme and its upstream flanking sequence has the potential to form an imperfect P_{zym} (Figure 7B). In contrast to the Osa 1-3 ribozyme, which demonstrated a very low $f_{cleaved}$ in the context of its upstream flanking sequence, the Osa 1-8 upstream+ribozyme construct self-cleaved to nearly 0.60 within 30 min (Figure 8). This higher

than anticipated activity is likely due to the weak nature of the interactions between the ribozyme and upstream flanking sequence. Additionally, within the predicted structure for the Osa 1-8 upstream+ribozyme construct, the native ribozyme is already partially folded, with native pairings P3 and P4 predicted to form (Figure 7B). For the Osa 1-8 upstream+ribozyme+downstream construct, significant inhibition was observed at early timepoints but not at 180 min, reflecting somewhat lower self-cleavage in the presence of flanking sequences (Figure 8). Once again, the native P3 is predicted to fold in the presence of upstream and downstream flanking sequences of the Osa 1-8 ribozyme (Figure 7C). The presence of strong pairings within the ribozyme and weak interactions between the flanking sequences and the ribozyme may weaken P_{zym} and allow appreciable self-cleavage of the Osa 1-8 ribozyme.

During our analysis we also analyzed RNA-seq coverage of each ribozyme and its flanking sequences from published datasets to determine whether the ribozymes cleaved *in vivo*. Consistent with previous findings using RT-PCR,[10] the Osa 1-2 ribozyme appears to cleave *in vivo*, as seen by the sharp decrease in coverage at the cleavage site of the ribozyme (Figure S1B). This *in vivo* activity also substantiates *in vitro* findings that the upstream and downstream flanks around the Osa 1-2 ribozyme form self-structures that permit folding and cleavage of the ribozyme (Figure 2B). Furthermore, we found that sequences in P_{up} and P_{down} were conserved across different rice cultivars, suggesting there is selective pressure to maintain these sequences.

Interestingly, we also found evidence of self-cleavage for the Osa 1-3 and Osa 1-8 ribozymes in root tissue (Figure S1D, S1F). This contrasts with their inhibition observed *in vitro*. Understanding the differences that *in vitro* and *in vivo* environments have on the ability of flanking sequence to regulate ribozyme activity will be essential for understanding their native role in rice and employment in synthetic applications. Similar to how riboswitches alter conformation in

response to changing concentrations of cellular metabolites, interactions between a ribozyme and its flanking sequences may change in the cellular milieu. For instance, differences in the rates of transcription *in vitro* and *in vivo* may account for some of the discrepancies in cleavage activity for the Osa 1-3 and Osa 1-8 ribozymes. The T7 polymerase used in our co-transcriptional cleavage assays is derived from phage T7 and has an elongation rate of ~15 kb/min,[63] while typical eukaryotic polymerases have an elongation rate that is 15 to 3 times slower, at 1-6 kb/min.[64] Additionally, binding of other macromolecules such as proteins could be responsible for alleviating ribozyme inhibition in vivo. Chaperone proteins, for instance, can assist in refolding small self-cleaving ribozymes, contributing to their regulation.[65–67] Indeed, the highly variable P3 extension of twister ribozymes[12,13,15] could provide an access point for a protein to bind. Furthermore, the presence of metabolites could alter the stability and rate of self-cleavage for the ribozyme. For instance, kinetic studies of ribozymes in the presence of glutamate-chelated magnesium enhanced the rate of self-cleavage for the human CPEB3 ribozyme by 1.6-fold.[68] In the case of twister ribozymes, small molecules in the buffer have also been found to enhance the self-cleavage rate up to 5-fold by shuttling protons to the active site.[20,69] Such catalysis has also been shown to rescue ribozymes that would otherwise be inactive.[69] Furthermore, experiments performed in media containing the 15 most abundant metabolites of *E. coli*, which comprise 80% of the *E. coli* metabolome, demonstrated a decrease in thermodynamic stability and an increase in chemical stability (i.e. resistance to degradation) for a series of structured RNAs (the guanine aptamer, the CPEB3 ribozyme, and $tRNA^{Phe}$) of ~2- to ~10-fold relative to standard *in vitro* conditions, such as 2 mM free Mg^{2+} and 25 mM free Mg^{2+}.[70] Such changes could favor conformations other than P_{zym} for the Osa 1-3 and Osa 1-8 ribozymes. It is also possible that the ribozymes may self-cleave to some extent during extraction or library preparation. Further

experiments are needed to identify more clearly the cause of the difference in activity between *in vitro* and *in vivo* conditions.

When designing synthetic constructs that involve small self-cleaving ribozymes, flanking sequence must be taken into consideration. For applications necessitating an active twister ribozyme, P_{up} and P_{down} could be designed and positioned adjacent to the ribozyme to promote self-cleavage. Conversely, if an inactive ribozyme is desired, a ribozyme-complementary region could be placed upstream of the ribozyme to create a P_{zym} as seen for the Osa 1-3 ribozyme. Specifically, for applications in cells, controls to ensure that cellular conditions do not alter self-cleavage efficiency would be necessary. For inactivated ribozymes, activity could be selectively turned on by addition of an ASO or another type of activating signal. In sum, flanking sequence affords new opportunities for controlled manipulation of ribozyme activity.

Overall, our analysis demonstrates that rice twister ribozymes are differentially regulated via flanking sequences. It may be that such inhibition regulates RNA processing and that certain activators, whether natural ASOs or proteins, alleviate it. Ultimately, understanding how these ribozymes are regulated in rice should provide a deeper understanding of their native role. More generally, flanking sequences provide a local means for regulating the function of any RNA. This has relevance for both gene regulation and synthetic biology where ribozymogens could be activated in specific tissues by existing RNAs or therapeutic ASOs.

ASSOCIATED CONTENT

The following files are available free of charge.

Supporting Information Available: Supplementary tables about genetic context, sequences studied, and p-values, as well as Supplementary figures including *in vivo* expression data, gels from in-line probing and co-transcriptional cleavage assays, sequence alignments, and melt data.

AUTHOR INFORMATION

Corresponding Author

***Philip C. Bevilacqua** – Department of Chemistry, Center for RNA Molecular Biology and Department of Biochemistry and Molecular Biology, Pennsylvania State University, University Park, Pennsylvania 16802, United States; orcid.org/0000-0001-8074-3434; Email: pcb5@psu.edu

Author Contributions

The manuscript was written with contributions from all authors. All authors have given approval to the final version of the manuscript.

Funding Sources

This work was supported by a HITS seed grant provided by Huck Institutes of Life Sciences at Penn State. Additional funding was provided by U.S. National Science Foundation grant IOS-2122357.

ACKNOWLEDGMENTS

The authors thank Dr. Jacob Sieg and Dr. Elizabeth Jolley for conversations about ILP and helpful suggestions regarding the manuscript, as well as Kobie Kirven for advice on bioinformatics.

ABBREVIATIONS

AS antisense transcripts; ASO, antisense oligonucleotide; DNA, deoxyribonucleic acid; ILP, in-line probing; PAGE, polyacrylamide gel electrophoresis; PK, pseudoknot; RNA, ribonucleic acid.

References

(1) Bevilacqua, P. C.; Ritchey, L. E.; Su, Z.; Assmann, S. M. Genome-Wide Analysis of RNA Secondary Structure. *Annu. Rev. Genet.* **2016**, *50*, 235–266.

(2) Jimenez, R. M.; Polanco, J. A.; Lupták, A. Chemistry and Biology of Self-Cleaving Ribozymes. *Trends Biochem. Sci.* **2015**, *40*, 648–661.

(3) Weinberg, C. E.; Weinberg, Z.; Hammann, C. Novel Ribozymes: Discovery, Catalytic Mechanisms, and the Quest to Understand Biological Function. *Nucleic Acids Res.* **2019**, *47*, 9480–9494.

(4) Prody, G. A.; Bakos, J. T.; Buzayan, J. M.; Schneider, I. R.; Bruening, G. Autolytic Processing of Dimeric Plant Virus Satellite RNA. *Science* **1986**, *231*, 1577–1580.

(5) Buzayan, J. M.; Gerlach, W. L.; Bruening, G. Non-Enzymatic Cleavage and Ligation of RNAs Complementary to a Plant Virus Satellite RNA. *Nature* **1986**, *323*, 349–353.

(6) Kuo, M. Y.; Sharmeen, L.; Dinter-Gottlieb, G.; Taylor, J. Characterization of Self-Cleaving RNA Sequences on the Genome and Antigenome of Human Hepatitis Delta Virus. *J. Virol.* **1988**, *62*, 4439–4444.

(7) Saville, B. J.; Collins, R. A. A Site-Specific Self-Cleavage Reaction Performed by a Novel RNA in *Neurospora* Mitochondria. *Cell* **1990**, *61*, 685–696.

(8) Winkler, W. C.; Nahvi, A.; Roth, A.; Collins, J. A.; Breaker, R. R. Control of Gene Expression by a Natural Metabolite-Responsive Ribozyme. *Nature* **2004**, *428*, 281–286.

(9) Salehi-Ashtiani, K.; Lupták, A.; Litovchick, A.; Szostak, J. W. A Genomewide Search for Ribozymes Reveals an HDV-Like Sequence in the Human *CPEB3* Gene. *Science* **2006**, *313*, 1788–1792.

(10) Roth, A.; Weinberg, Z.; Chen, A. G. Y.; Kim, P. B.; Ames, T. D.; Breaker, R. R. A Widespread Self-Cleaving Ribozyme Class Is Revealed by Bioinformatics. *Nat. Chem. Biol.* **2014**, *10*, 56–60.

(11) Weinberg, Z.; Kim, P. B.; Chen, T. H.; Li, S.; Harris, K. A.; Lünse, C. E.; Breaker, R. R. New Classes of Self-Cleaving Ribozymes Revealed by Comparative Genomics Analysis. *Nat. Chem. Biol.* **2015**, *11*, 606–610.

(12) Gebetsberger, J.; Micura, R. Unwinding the Twister Ribozyme: From Structure to Mechanism. *WIREs RNA* **2017**, *8*, e1402.

(13) Eiler, D.; Wang, J.; Steitz, T. A. Structural Basis for the Fast Self-Cleavage Reaction Catalyzed by the Twister Ribozyme. *Proc. Natl. Acad. Sci.* **2014**, *111*, 13028–13033.

(14) Liu, Y.; Wilson, T. J.; McPhee, S. A.; Lilley, D. M. J. Crystal Structure and Mechanistic Investigation of the Twister Ribozyme. *Nat. Chem. Biol.* **2014**, *10*, 739–744.

(15) Ren, A.; Košutić, M.; Rajashankar, K. R.; Frener, M.; Santner, T.; Westhof, E.; Micura, R.; Patel, D. J. In-Line Alignment and Mg2+ Coordination at the Cleavage Site of the Env22 Twister Ribozyme. *Nat. Commun.* **2014**, *5*, 5534.

(16) Vušurović, N.; Altman, R. B.; Terry, D. S.; Micura, R.; Blanchard, S. C. Pseudoknot Formation Seeds the Twister Ribozyme Cleavage Reaction Coordinate. *J. Am. Chem. Soc.* **2017**, *139*, 8186–8193.

(17) Wilson, T. J.; Liu, Y.; Domnick, C.; Kath-Schorr, S.; Lilley, D. M. J. The Novel Chemical Mechanism of the Twister Ribozyme. *J. Am. Chem. Soc.* **2016**, *138*, 6151–6162.

(18) Kobori, S.; Yokobayashi, Y. High-Throughput Mutational Analysis of a Twister Ribozyme. *Angew. Chem. Int. Ed.* **2016**, *55*, 10354–10357.

(19) Roberts, J. M.; Beck, J. D.; Pollock, T. B.; Bendixsen, D. P.; Hayden, E. J. RNA Sequence to Structure Analysis from Comprehensive Pairwise Mutagenesis of Multiple Self-Cleaving Ribozymes. *eLife* **2023**, *12*, e80360.

(20) Messina, K. J.; Bevilacqua, P. C. Cellular Small Molecules Contribute to Twister Ribozyme Catalysis. *J. Am. Chem. Soc.* **2018**, *140*, 10578–10582.

(21) Jolley, E. A.; Bormes, K. M.; Bevilacqua, P. C. Upstream Flanking Sequence Assists Folding of an RNA Thermometer. *J. Mol. Biol.* **2022**, *434*, 167786.

(22) Williams, A. M.; Dickson, T. M.; Lagoa-Miguel, C. A.; Bevilacqua, P. C. Biological Solution Conditions and Flanking Sequence Modulate LLPS of RNA G-Quadruplex Structures. *RNA* **2022**, *28*, 1197–1209.

(23) Woodson, S. A.; Cech, T. R. Alternative Secondary Structures in the 5' Exon Affect Both Forward and Reverse Self-Splicing of the *Tetrahymena* Intervening Sequence RNA. *Biochemistry* **1991**, *30*, 2042–2050.

(24) Pan, J.; Woodson, S. A. Folding Intermediates of a Self-Splicing RNA: Mispairing of the Catalytic Core. *J. Mol. Biol.* **1998**, *280*, 597–609.

(25) Heilman-Miller, S. L.; Woodson, S. A. Effect of Transcription on Folding of the *Tetrahymena* Ribozyme. *RNA* **2003**, *9*, 722–733.

(26) Chadalavada, D. M.; Knudsen, S. M.; Nakano, S.; Bevilacqua, P. C. A Role for Upstream RNA Structure in Facilitating the Catalytic Fold of the Genomic Hepatitis Delta Virus Ribozyme. *J. Mol. Biol.* **2000**, *301*, 349–367.

(27) Liu, G.; Jiang, H.; Sun, W.; Zhang, J.; Chen, D.; Murchie, A. I. H. The Function of Twister Ribozyme Variants in Non-LTR Retrotransposition in *Schistosoma Mansoni*. *Nucleic Acids Res.* **2021**, *49*, 10573–10588.

(28) Fukagawa, N. K.; Ziska, L. H. Rice: Importance for Global Nutrition. *J. Nutr. Sci. Vitaminol. (Tokyo)* **2019**, *65*, S2–S3.

(29) Liu, W.; Wang, G.-L. Plant Innate Immunity in Rice: A Defense against Pathogen Infection. *Natl. Sci. Rev.* **2016**, *3*, 295–308.

(30) Nalley, L.; Tsiboe, F.; Durand-Morat, A.; Shew, A.; Thoma, G. Economic and Environmental Impact of Rice Blast Pathogen (*Magnaporthe oryzae*) Alleviation in the United States. *PLOS ONE* **2016**, *11* (12), e0167295.

(31) Singh, P.; Mazumdar, P.; Harikrishna, J. A.; Babu, S. Sheath Blight of Rice: A Review and Identification of Priorities for Future Research. *Planta* **2019**, *250*, 1387–1407.

(32) Cunningham, F.; Allen, J. E.; Allen, J.; Alvarez-Jarreta, J.; Amode, M. R.; Armean, I. M.; Austine-Orimoloye, O.; Azov, A. G.; Barnes, I.; Bennett, R.; Berry, A.; Bhai, J.; Bignell, A.; Billis, K.; Boddu, S.; Brooks, L.; Charkhchi, M.; Cummins, C.; Da Rin Fioretto, L.; Davidson, C.; Dodiya, K.; Donaldson, S.; El Houdaigui, B.; El Naboulsi, T.; Fatima, R.; Giron, C. G.; Genez, T.; Martinez, J. G.; Guijarro-Clarke, C.; Gymer, A.; Hardy, M.; Hollis, Z.; Hourlier, T.; Hunt, T.; Juettemann, T.; Kaikala, V.; Kay, M.; Lavidas, I.; Le, T.; Lemos, D.; Marugán, J. C.; Mohanan, S.; Mushtaq, A.; Naven, M.; Ogeh, D. N.; Parker, A.; Parton, A.; Perry, M.; Piližota, I.; Prosovetskaia, I.; Sakthivel, M. P.; Salam, A. I. A.; Schmitt, B. M.; Schuilenburg, H.; Sheppard, D.; Pérez-Silva, J. G.; Stark, W.; Steed, E.; Sutinen, K.; Sukumaran, R.; Sumathipala, D.; Suner, M.-M.; Szpak, M.; Thormann, A.; Tricomi, F. F.; Urbina-Gómez, D.; Veidenberg, A.; Walsh, T. A.; Walts, B.; Willhoft, N.; Winterbottom, A.; Wass, E.; Chakiachvili, M.; Flint, B.; Frankish, A.; Giorgetti, S.; Haggerty, L.; Hunt, S. E.; IIsley, G. R.; Loveland, J. E.; Martin, F. J.; Moore, B.; Mudge, J. M.; Muffato, M.; Perry, E.; Ruffier, M.; Tate, J.; Thybert, D.; Trevanion, S. J.; Dyer, S.;

Harrison, P. W.; Howe, K. L.; Yates, A. D.; Zerbino, D. R.; Flicek, P. Ensembl 2022. *Nucleic Acids Res.* **2022**, *50*, D988–D995.

(33) Zheng, X.; Yang, J.; Zhou, C.; Zhang, C.; Zhang, Q.; Wei, X. Allosteric DNAzyme-Based DNA Logic Circuit: Operations and Dynamic Analysis. *Nucleic Acids Res.* **2019**, *47*, 1097–1109.

(34) Felletti, M.; Stifel, J.; Wurmthaler, L. A.; Geiger, S.; Hartig, J. S. Twister Ribozymes as Highly Versatile Expression Platforms for Artificial Riboswitches. *Nat. Commun.* **2016**, *7* (1), 12834.

(35) Sakai, H.; Lee, S. S.; Tanaka, T.; Numa, H.; Kim, J.; Kawahara, Y.; Wakimoto, H.; Yang, C.; Iwamoto, M.; Abe, T.; Yamada, Y.; Muto, A.; Inokuchi, H.; Ikemura, T.; Matsumoto, T.; Sasaki, T.; Itoh, T. Rice Annotation Project Database (RAP-DB): An Integrative and Interactive Database for Rice Genomics. *Plant Cell Physiol.* **2013**, *54*, e6–e6.

(36) Kawahara, Y.; de la Bastide, M.; Hamilton, J. P.; Kanamori, H.; McCombie, W. R.; Ouyang, S.; Schwartz, D. C.; Tanaka, T.; Wu, J.; Zhou, S.; Childs, K. L.; Davidson, R. M.; Lin, H.; Quesada-Ocampo, L.; Vaillancourt, B.; Sakai, H.; Lee, S. S.; Kim, J.; Numa, H.; Itoh, T.; Buell, C. R.; Matsumoto, T. Improvement of the Oryza Sativa Nipponbare Reference Genome Using next Generation Sequence and Optical Map Data. *Rice* **2013**, *6*, 4.

(37) Altschul, S. F.; Gish, W.; Miller, W.; Myers, E. W.; Lipman, D. J. Basic Local Alignment Search Tool. *J. Mol. Biol.* **1990**, *215*, 403–410.

(38) O'Leary, N. A.; Wright, M. W.; Brister, J. R.; Ciufo, S.; Haddad, D.; McVeigh, R.; Rajput, B.; Robbertse, B.; Smith-White, B.; Ako-Adjei, D.; Astashyn, A.; Badretdin, A.; Bao, Y.; Blinkova, O.; Brover, V.; Chetvernin, V.; Choi, J.; Cox, E.; Ermolaeva, O.; Farrell, C. M.;

Goldfarb, T.; Gupta, T.; Haft, D.; Hatcher, E.; Hlavina, W.; Joardar, V. S.; Kodali, V. K.; Li, W.; Maglott, D.; Masterson, P.; McGarvey, K. M.; Murphy, M. R.; O'Neill, K.; Pujar, S.; Rangwala, S. H.; Rausch, D.; Riddick, L. D.; Schoch, C.; Shkeda, A.; Storz, S. S.; Sun, H.; Thibaud-Nissen, F.; Tolstoy, I.; Tully, R. E.; Vatsan, A. R.; Wallin, C.; Webb, D.; Wu, W.; Landrum, M. J.; Kimchi, A.; Tatusova, T.; DiCuccio, M.; Kitts, P.; Murphy, T. D.; Pruitt, K. D. Reference Sequence (RefSeq) Database at NCBI: Current Status, Taxonomic Expansion, and Functional Annotation. *Nucleic Acids Res.* **2016**, *44*, D733–D745.

(39) Chen, S.; Zhou, Y.; Chen, Y.; Gu, J. Fastp: An Ultra-Fast All-in-One FASTQ Preprocessor. *Bioinformatics* **2018**, *34*, i884–i890.

(40) Kim, D.; Paggi, J. M.; Park, C.; Bennett, C.; Salzberg, S. L. Graph-Based Genome Alignment and Genotyping with HISAT2 and HISAT-Genotype. *Nat. Biotechnol.* **2019**, *37*, 907–915.

(41) Danecek, P.; Bonfield, J. K.; Liddle, J.; Marshall, J.; Ohan, V.; Pollard, M. O.; Whitwham, A.; Keane, T.; McCarthy, S. A.; Davies, R. M.; Li, H. Twelve Years of SAMtools and BCFtools. *GigaScience* **2021**, *10*, giab008.

(42) Mansueto, L.; Fuentes, R. R.; Borja, F. N.; Detras, J.; Abriol-Santos, J. M.; Chebotarov, D.; Sanciangco, M.; Palis, K.; Copetti, D.; Poliakov, A.; Dubchak, I.; Solovyev, V.; Wing, R. A.; Hamilton, R. S.; Mauleon, R.; McNally, K. L.; Alexandrov, N. Rice SNP-Seek Database Update: New SNPs, Indels, and Queries. *Nucleic Acids Res.* **2017**, *45*, D1075–D1081.

(43) Sievers, F.; Higgins, D. G. Clustal Omega, Accurate Alignment of Very Large Numbers of Sequences. In *Multiple Sequence Alignment Methods*; Russell, D. J., Ed.; Methods in Molecular Biology; Humana Press: Totowa, NJ, 2014; Vol. 1079, 105–116.

(44) Proctor, J. R.; Meyer, I. M. CoFold : An RNA Secondary Structure Prediction Method That Takes Co-transcriptional Folding into Account. *Nucleic Acids Res.* **2013**, *41*, e102–e102.

(45) Weinberg, Z.; Breaker, R. R. R2R - Software to Speed the Depiction of Aesthetic Consensus RNA Secondary Structures. *BMC Bioinformatics* **2011**, *12*, 3.

(46) Reuter, J. S.; Mathews, D. H. RNAstructure: Software for RNA Secondary Structure Prediction and Analysis. *BMC Bioinformatics* **2010**, *11*, 129.

(47) Újvári, A.; Martin, C. T. Evidence for DNA Bending at the T7 RNA Polymerase Promoter. *J. Mol. Biol.* **2000**, *295*, 1173–1184.

(48) Xu, J.; Henry, A.; Sreenivasulu, N. Rice Yield Formation under High Day and Night Temperatures—A Prerequisite to Ensure Future Food Security. *Plant Cell Environ.* **2020**, *43*, 1595–1608.

(49) Das, R.; Laederach, A.; Pearlman, S. M.; Herschlag, D.; Altman, R. B. SAFA: Semi-Automated Footprinting Analysis Software for High-Throughput Quantification of Nucleic Acid Footprinting Experiments. *RNA* **2005**, *11*, 344–354.

(50) Good, N. E.; Winget, G. D.; Winter, W.; Connolly, T. N.; Izawa, S.; Singh, R. M. M. Hydrogen Ion Buffers for Biological Research*. *Biochemistry* **1966**, *5*, 467–477.

(51) Chakraborty, P.; Acquasaliente, L.; Pelc, L. A.; Di Cera, E. Interplay between Conformational Selection and Zymogen Activation. *Sci. Rep.* **2018**, *8*, 4080.

(52) Bevilacqua, P. C.; Cerrone-Szakal, A. L.; Siegfried, N. A. Insight into the Functional Versatility of RNA through Model-Making with Applications to Data Fitting. *Q. Rev. Biophys.* **2007**, *40*, 55–85.

(53) Soukup, G. A.; Breaker, R. R. Relationship between Internucleotide Linkage Geometry and the Stability of RNA. *RNA* **1999**, *5*, 1308–1325.

(54) The Rice Chromosomes 11 and 12 Sequencing Consortia*. The Sequence of Rice Chromosomes 11 and 12, Rich in Disease Resistance Genes and Recent Gene Duplications. *BMC Biol.* **2005**, *3*, 20.

(55) Jeon, J.; Lee, G.-W.; Kim, K.-T.; Park, S.-Y.; Kim, S.; Kwon, S.; Huh, A.; Chung, H.; Lee, D.-Y.; Kim, C.-Y.; Lee, Y.-H. Transcriptome Profiling of the Rice Blast Fungus *Magnaporthe oryzae* and Its Host *Oryza sativa* During Infection. *Mol. Plant-Microbe Interactions.* **2020**, *33*, 141–144.

(56) Zhang, D. Y.; Seelig, G. Dynamic DNA Nanotechnology Using Strand-Displacement Reactions. *Nat. Chem.* **2011**, *3*, 103–113.

(57) Zhang, Q.-L.; Wang, L.-L.; Liu, Y.; Lin, J.; Xu, L. A Kinetically Controlled Platform for Ligand-Oligonucleotide Transduction. *Nat. Commun.* **2021**, *12*, 4654.

(58) Vazquez-Anderson, J.; Contreras, L. M. Regulatory RNAs: Charming Gene Management Styles for Synthetic Biology Applications. *RNA Biol.* **2013**, *10*, 1778–1797.

(59) McCown, P. J.; Corbino, K. A.; Stav, S.; Sherlock, M. E.; Breaker, R. R. Riboswitch Diversity and Distribution. *RNA* **2017**, *23*, 995–1011.

(60) Assmann, S. M.; Chou, H.-L.; Bevilacqua, P. C. Rock, Scissors, Paper: How RNA Structure Informs Function. *Plant Cell* **2023**, *35*, 1671–1707.

(61) Chan, L.; Yokota, T. Development and Clinical Applications of Antisense Oligonucleotide Gapmers. In *Gapmers*; Yokota, T., Maruyama, R., Eds.; Methods in Molecular Biology; Springer US: New York, NY, 2020; Vol. 2176, 21–47.

(62) Rinaldi, C.; Wood, M. J. A. Antisense Oligonucleotides: The next Frontier for Treatment of Neurological Disorders. *Nat. Rev. Neurol.* **2018**, *14*, 9–21.

(63) Sastry, S. S.; Ross, B. M. Nuclease Activity of T7 RNA Polymerase and the Heterogeneity of Transcription Elongation Complexes. *J. Biol. Chem.* **1997**, *272*, 8644–8652.

(64) Jonkers, I.; Lis, J. T. Getting up to Speed with Transcription Elongation by RNA Polymerase II. *Nat. Rev. Mol. Cell Biol.* **2015**, *16*, 167–177.

(65) Herschlag, D.; Khosla, M.; Tsuchihashi, Z.; Karpel, R. L. An RNA Chaperone Activity of Non-Specific RNA Binding Proteins in Hammerhead Ribozyme Catalysis. *EMBO J.* **1994**, *13*, 2913–2924.

(66) Herschlag, D. RNA Chaperones and the RNA Folding Problem. *J. Biol. Chem.* **1995**, *270*, 20871–20874.

(67) Ruminski, D. J.; Watson, P. Y.; Mahen, E. M.; Fedor, M. J. A DEAD-Box RNA Helicase Promotes Thermodynamic Equilibration of Kinetically Trapped RNA Structures in Vivo. *RNA* **2016**, *22*, 416–427.

(68) Yamagami, R.; Bingaman, J. L.; Frankel, E. A.; Bevilacqua, P. C. Cellular Conditions of Weakly Chelated Magnesium Ions Strongly Promote RNA Stability and Catalysis. *Nat. Commun.* **2018**, *9*, 2149.

(69) Messina, K. J.; Kierzek, R.; Tracey, M. A.; Bevilacqua, P. C. Small Molecule Rescue and Glycosidic Conformational Analysis of the Twister Ribozyme. *Biochemistry* **2019**, *58*, 4857–4868.

(70) Sieg, J. P.; McKinley, L. N.; Huot, M. J.; Yennawar, N. H.; Bevilacqua, P. C. The Metabolome Weakens RNA Thermodynamic Stability and Strengthens RNA Chemical Stability. *Biochemistry* **2022**, *61*, 2579–2591.

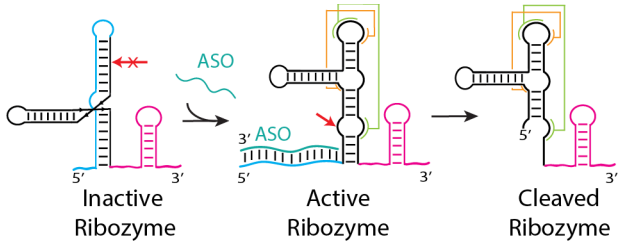

“For Table of Contents Use Only”